FLUORESCENT IMPLANTABLE ELASTOMER TAGS FOR THE MEASURMENT OF OXYGEN IN INSECTS

by

Anne Burnett Robertson

B.Sc., Mount Allison University, 2015

A THESIS SUBMITTED IN PARTIAL FULFILLMENT OF
THE REQUIREMENTS FOR THE DEGREE OF

MASTER OF SCIENCE

in

The Faculty of Graduate and Postdoctoral Studies

(Zoology)

THE UNIVERSITY OF BRITISH COLUMBIA

(Vancouver)

July 2017

Abstract

Implantable fibre-optic probes are commonly used to measure the oxygen partial pressure (PO_2) within the haemolymph and tissues of insects, but they are highly invasive and traumatic. Furthermore, they can only measure the PO_2 of one spot of the insect's body at a time.

The objective of this thesis was to develop Fluorescent Implantable Elastomer Tags (FIETs) as an alternative to fibre-optic probes. These FIETs were characterized in terms of their uniformity in size, response to PO_2 and photodegradation. I assessed their viability for *in vivo* measurements by testing them in an autofluorescent system *in situ*.

I constructed a microfluidic chip to produce the FIETs, and characterized their uniformity. To establish the FIETs response to PO_2, they were exposed to oxygen (O_2) gas in nitrogen, ranging from 0 to 0.2 atm O_2. Holding the FIETs within steady-state environments of 0, 0.1 and 0.2 atm O_2 and constantly illuminating them for 60 seconds with the excitation light source determined the degree of photodegradation. The FIETs were tested within an autofluorescent system by creating an O_2 gradient within a block of 0.5% (w/v) agar.

My results indicate that 72% of the emulsions produced by the microfluidic chip are highly uniform when 1% sodium dodecyl sulfate (SDS) in water is used as the continuous phase. In comparison, only 55% of emulsions are highly uniform when 5% Kolliphor in water is used. FIET diameters ranged from 110 – 401 μm for 1% SDS and 67-120 μm for 5% Kolliphor. The FIETs exhibit a linear response to PO_2 (R^2=0.963), which is improved when fluorescence is normalized to fluorescence in anoxia (R^2=0.983). Photodegradation occurred over 60 seconds, causing a 31.6%, 6.1% and 359.7% drift in measured PO_2 within

0.2, 0.1 and 0.02 atm O_2 respectively. The FIETs were able to detect an O_2 gradient within 0.5% agar.

These results suggest that the FIETs are a viable option for measuring O_2 in insects *in vivo*, although improvements can be made to the uniformity and photostability of the FIETS. Future work should focus on the FIETs response to confounding factors such as temperature.

Lay abstract

Current methods for measuring the level of oxygen within the blood and tissues of small animals, such as insects, are highly invasive and harmful. My research developed micro-sized, implantable sensors that will provide a more accurate and less invasive method of monitoring oxygen within insects. These micro-sized sensors contain two fluorescent dyes: an indicator dye and a reference dye. Light transmitted into the insect's body stimulates these two dyes to fluoresce. The amount of fluorescent light emitted by the indicator dye changes as oxygen levels vary, while the fluorescence from the reference dye does not change. A microscope combined with a high-sensitivity imaging system compares the level of fluorescence from the two dyes to produce a signal indicating levels of internal oxygen. Development of these in-body sensors allows for a more complete understanding of insect respiratory systems, thereby improving understanding of the sub-lethal physiological responses of different insects to environmental conditions, including changing climate, pollution, and pesticides.

Preface

This is the original, unpublished research of the author, Anne Burnett Robertson.

Russ Algar, from the University of British Columbia, assisted with the selection of the reference dye within section 2.2.3. Hsin-Yun Tsai performed the addition of the reference dye and indicator dye to the polydimethylsiloxane base within section 2.2.3. Philip Matthews designed and printed the agar chamber used within section 2.5. I designed, constructed and operated the microfluidic chip. I also performed all of the FIET characterization tests. All analyses performed within ImageJ and R software are my own original work.

Table of contents

List of tables

List of figures

Acknowledgements

I must give a very special thank-you to my supervisor, Phil Matthews, who challenged and supported me through my research. Phil is not only a talented scientist, but he is also a wonderful teacher who always made time to help me understand the nuances of my thesis. Thank you to my committee members, Bill Milsom and Colin Brauner, for offering valuable feedback and making my committee meetings so enjoyable.

Russ Algar and Hsin-Yun Tsai from the UBC Chemistry department provided guidance in selecting the reference dye for this project. I am so grateful that they agreed to help me, particularly Hsin-Yun, who happily provided samples whenever I asked.

I would like to thank Daniel Lee for being an exemplary lab-mate. He is both a dedicated researcher and friend, always helping out around the lab with a positive attitude. A thank-you must also be given to Alex Chang and Ramen Ubdhi, who took excellent care of our insect colonies (so that we graduate students did not have to).

A special thank you to my family and friends who assuaged my stress and angst throughout this project. Especially Filip Jaworski, who listened to countless presentations and proposals with a smile on his face.

I am so grateful for the two years that I have spent within the UBC Zoology department. This is a truly unique and wonderful place to study, thank you to everyone in the department for making it so.

1: Introduction

1.1 The importance of insects and their respiratory physiology

Insects are biologically abundant and diverse – they have a valid species count of over one million, and unofficial estimates reach up to 5.5 million (Stork et al., 2015). The majority of these species perform important roles in ecosystems, acting as detritivores, herbivores, pollinators, predators and ecosystem engineers (Weisser and Siemann, 2013). Although the significance of insects in ecosystem function has been dismissed in the past, researchers are increasingly drawing attention to their impact on nutrient cycling, plant species richness and plant species diversity (Bagchi et al., 2014; Yang and Gratton, 2014). Insect herbivores directly impact plant species richness and diversity through phytophagy, which may be mutualistic or antagonistic (Weisser and Siemann, 2013). However, detritivores and saproxylic insects have a less direct route of impact; they feed off of dead and decaying matter, thereby releasing nutrients back to the soil for living plants to use (Jörg et al., 2016; Weisser and Siemann, 2013).

Not only are insects ecologically important, but they also have a profound effect on human wellbeing. For instance, the free pollination services provided by insects contribute to food security: seventy-five percent of global food crops and eighty percent of wild plant species are directly dependent on pollinator insects (Klatt et al., 2014; Le Conte and Navajas, 2008). However, insects also have the ability to negatively impact human health and economy. Mosquitoes are an example of a disease vector that people encounter on a daily basis in some regions of the world, exposing them to diseases such as Chikungunya virus, dengue virus, yellow fever, malaria and *Dirofilaria* parasites (Reiter, 2014). Insects can also impact the economy mainly as agricultural pests. In Brazil, the government loses an

estimated twelve billion US dollars every year to food pests (Oliveira et al., 2013). Household pests can also negatively impact tourism and economy. Australia experienced a 4,500 percent increase in bed bug infestations from 2000 to 2006, costing an estimated 100 million Australian dollars in management and treatment for the year of 2006 (Doggett et al., 2011; Doggett and Russell, 2008).

Both the positive and negative impacts of insects on human society will be affected in the future by climate change, globalization and pesticide use. In recent years the plight of the honeybee has received increased media attention, as wild colonies in both the United States and Europe have almost completely collapsed (Potts et al., 2010). The combined forces of increased pesticide use, climate change and habitat loss will continue to threaten pollinators' existence in the future (Potts et al., 2010). While society risks losing the benefits of pollinators, the negative effects of insects on human economy and health will only be amplified as climate change and globalization continue. Already, the zika virus - which is carried by the *Aedes aegypti* mosquito - has spread from Africa to Asia, Europe and Latin America (Dyer, 2015). The zika virus has been associated with an increase of microcephaly in newborn infants in Brazil, and is predicted to spread further north due to increased tourism, world trade, and climate change (Dyer, 2015; Kilpatrick and Randolph). An expansion towards northern latitudes is also predicted for members of the subfamily triatominae (commonly known as kissing bugs), which carry the protozoan responsible for Chagas disease (Lambert et al., 2008).

In spite of the major impacts that insects have on human health and society, relatively little is known regarding important aspects of their physiology, particularly their respiratory and acid-base systems. Knowledge of these systems could be useful in identifying

bioindicators. For example, is the respiratory system of a certain insect compromised following exposure to a pollutant? There are numerous insects currently used as bioindicators to determine the health of aquatic ecosystems, but only a few species have been identified for terrestrial environments (Hodkinson and Jackson, 2005). In addition, knowledge of insect respiration could be used in developing new pesticides to target harmful vectors of disease. For instance, increased resistance to phosphine insecticides is associated with lower respiration rates in several genera of grain beetles, but the mechanism of resistance has not been elucidated (Pimentel et al., 2007). Knowledge of insect respiration could be also used to protect endangered pollinators: sublethal doses of the insecticide Imidacloprid have been shown to adversely affect honeybees' gas exchange rhythm, but Imidacloprid's mechanism of action is not fully understood (Hatjina et al., 2013). Understanding how oxygen (O_2) moves through the respiratory system is important for explaining how insect respiratory systems function, and could shed light on mechanisms of pesticide resistance and toxicity. Currently, two technologies are commonly used for the direct measurement of O_2 partial pressure (PO_2) within insects: Clark electrodes and fibre-optic probes. Both of these technologies have drawbacks with their use, and it has previously been noted that development of an implantable sensor system would produce more accurate results (Harrison, 2001).

1.2 Current knowledge of insect respiration and future directions

Insect respiration begins with small openings in the insect's body called spiracles, that allow for the exchange of gases between the atmosphere and the insect (Matthews and Terblanche, 2015). Spiracles open into a system of cuticle-lined tubes known as tracheae,

which lead to a network of increasingly smaller, blind-ending tracheoles that taper to 0.1 μm or less in diameter (Chapman, 2013; Groenewald et al., 2012; Wigglesworth, 1930). These tracheoles are the main site of gas exchange, providing approximately 90% of the lateral diffusing capacity of the tracheal system (Snelling et al., 2011). Due to their small size, the tracheoles lie in close proximity to the cells, thus reducing the distance that O_2 must diffuse to reach the mitochondria (Chapman, 2013). In flight muscles the tracheoles may even indent the plasma membrane, although they do not penetrate the cells (Chapman, 2013).

The tracheae are filled with air, through which O_2 diffuses much more quickly than water; the diffusion coefficient ($m^2 \cdot s^{-1}$) of O_2 in air is 10,000 times higher than in water (Harrison et al., 2012). The ends of the tracheoles are filled with water in resting insects, but it has been shown that this liquid may be replaced with air during periods of hypoxia (Wigglesworth, 1930). It has also been shown that the proportion of liquid in the tracheoles decreases as ambient O_2 decreases (Wigglesworth, 1935).

O_2 and carbon dioxide (CO_2) move through the insect tracheal system via diffusion, convection or a combination of both. Diffusion refers to the movement of molecules from areas of high free energy to areas of low free energy, whereas convection refers to the movement of molecules from an area of high pressure to an area of lower pressure. Both diffusion and convection contribute to gas exchange within the insect respiratory system. For example, CO_2 diffuses from the tracheoles to the spiracles as it leaves the body while O_2 diffuses in the opposite direction as it enters (Harrison et al., 2012). While diffusion is a passive process, insects have some control over convection through their tracheal system by coordinating abdominal contractions with spiracular opening (Groenewald et al., 2012; Harrison et al., 2012). Previous studies have shown that hypoxic conditions can stimulate a

higher frequency of abdominal contractions in order to increase the airflow through the tracheal system and O_2 delivery to the tissues (Greenlee and Harrison, 2004). Similarly, hypercapnic conditions also increase the frequency of abdominal and spiracular contractions in insects (Harrison, 1989).

Insects display a range of gas exchange patterns through a combination of abdominal contractions and spiracular opening. These breathing patterns have been shown to vary between species, as well as between individuals within a species (Inder and Duncan, 2015). The two most common patterns are continuous and discontinuous gas exchange, although insects may also display patterns that are a blend of discontinuous and continuous gas exchange (Matthews and Terblanche, 2015). Continuous gas exchange refers to when the insect's spiracles remain open, which allows for the constant exchange of CO_2 and O_2 between the insect and the atmosphere (Matthews and Terblanche, 2015). Discontinuous gas exchange cycles (DGCs) are a pattern of respiration that consists of three phases: closed phase, flutter phase and open phase (Harrison et al., 2012; Matthews and White, 2011a). During the closed phase the spiracles close, thus preventing uptake of O_2 and removal of CO_2 (Chapman, 2013). The flutter phase consists of rapid partial opening and closing of the spiracles, during this period O_2 is able to diffuse from the atmosphere into the tracheal system but relatively little CO_2 escapes from the insect (Chapman, 2013). In the final stage of DGC, the open phase, the spiracles open and CO_2 is removed while O_2 is taken up (Chapman, 2013).

Although gas exchange patterns and the anatomy of the insect respiratory system have been well characterized, many aspects of insect respiration and physiology remain unknown, particularly within smaller species. The interspecific body size distribution of

insects is large – the smallest member (*Dicopomorpha echmepterygis*) measures 139 μm in body length, while the largest (*Phobaeticus chani*) measures 357 mm, over 2,500 times longer (Gaston and Chown, 2013; Rainford et al., 2016). Due to the large size of fibre-optic probes, researchers have been limited to either using insects at the larger end of the spectrum (such as cockroaches or locusts) or using respirometry chambers to measure CO_2 emission and then infer insects' physiological state. Overall, there is a lack of research providing direct measurements of physiological O_2 in smaller insects.

For example, the investigation of O_2 guarding within dampwood termites lacks direct measurements of gut PO_2 (Lighton and Ottesen, 2005). These lower-order termites subsist entirely upon damp wood and have formed a symbiotic relationship with obligate anaerobic protists. The protists are provided with an anaerobic environment in the termite's gut, where they break down lignin-cellulose of the wood that the termite would otherwise be unable to digest (Brune, 2014; Lighton and Ottesen, 2005). Previous research has used Clark microelectrodes to characterize the O_2 profile of termite guts *in situ* (Brune et al., 1995), but this has yet to be done *in vivo* due to the termites' small size. One study tested the hypothesis that dampwood termites use DGCs in hyperoxic conditions to exclude O_2 from their digestive tract (Lighton and Ottesen, 2005). To measure whether DGCs were occurring or not, a respirometry chamber was used to measure CO_2 emission (Lighton and Ottesen, 2005). From the CO_2 emission rates, spiracular opening, internal CO_2 and internal O_2 were inferred, but not quantified. This study concluded that dampwood termites engage in 'O_2 guarding' by maintaining partially closed spiracles in hyperoxia rather than adopting a DGC. But because of termites' small size, the researchers were unable to measure PO_2 directly within the

termites' guts. Without a direct measurement of gut PO_2, it is unknown how effective the termites' O_2 guarding strategy is. As Lighton and Ottensen (2005) said:

"Our investigation raises some questions. Primarily, what are the actual endotracheal PO_2 and PCO_2 levels during hyperoxia? Our results show that oxygen guarding exists, but do not quantify its effectiveness. On *a priori* grounds it is logical to assume that the limiting factor in oxygen guarding is the degree to which internal hypercapnia can be tolerated. In this respect, quantifying responses to graded hyperoxia would be interesting."

This study not only illustrates how quantifiable measurements of PO_2 are essential for research, it also shows how scientists' scope of research is limited by the size of the organism they are studying. For instance, often it is smaller insects that are used as bio-indicators to reflect the overall health of an ecosystem, but direct measurements of PO_2 are nearly impossible to measure due to their size. The phantom midge (*Chaoborus crystallinus*) is an example of a small bio-indicator used in freshwater ecosystems for the presence of heavy metals, such as cadmium and lead (Hare and Tessier, 1998; Hodkinson and Jackson, 2005). Changes in O_2 uptake and oxy-regulatory capacity are commonly measured within organisms as a reflection of sublethal stress. With a micro-sized, implantable sensor rather than a fibre-optic probe, measurements of PO_2 could be taken within *Chaoborus crystallinus* to quantify changes in O_2 uptake in the presence of heavy metals and hypoxic conditions (Brodersen et al., 2008). Direct measurements of PO_2 within the animal would allow for direct measurement of hypoxemia caused by either environmental stress or by pollutants.

In addition to a lack of research regarding respiration in smaller insects, there is a significant gap of knowledge regarding their gigantic ancestors. The current hypothesis for paleogigantism is that atmospheric PO_2 during the Permian and Carboniferous period was

hyperoxic compared to current levels, resulting in dragonflies with wingspans of up to seventy centimetres and millipedes with body lengths of up to two metres (Dudley, 1998; Harrison et al., 2010; Niven et al., 2007; VandenBrooks et al., 2012). This theory also contends that the decrease in atmospheric PO_2 during the Triassic period caused the extinction of gigantic insect species and limited the size of the surviving ones (Harrison et al., 2010).

An explicit assumption of this theory is that atmospheric PO_2 limits insect body size due to their tracheal system. O_2 has to diffuse across larger distances in the blind-ending tracheoles of giant insects, so intuitively it would seem that hyperoxia allows for larger body size. However, other research has contended that the Paleozoic O_2 pulse did not necessarily cause gigantism (VandenBrooks et al., 2012). While significant correlations have been found between atmospheric PO_2 and insect body size, there are periods of uncoupling (when gigantism persists despite a drop in atmospheric O_2, or when insects remain small despite an O_2 pulse) which have caused researchers to seek other explanations. An alternative theory points out that one period of uncoupling takes place during the diversification of birds (the early Cretaceous), and that predation may have a stronger influence on body size rather than atmospheric PO_2 (Clapham and Karr, 2012). Other researchers have noted that although atmospheric PO_2 seems to constrain body size for larger individuals, there are relatively few studies that control for confounding factors, such as temperature or life stage (Harrison et al., 2010). Many questions surrounding insect evolution and the Paleozoic O_2 pulse could be investigated using implantable O_2 sensors. These sensors could be implanted at different points along the trachea of large and small insects to determine if distance limits O_2 delivery. Furthermore, the sensors could be placed within different tissues to see if PO_2 decreases in

tissues further from the spiracle, thus providing evidence either for or against O_2 as a constraint on body size.

In all of the above examples – O_2 guarding, bioindicators and paleogigantism – there are clear gaps in knowledge involving O_2 and insect respiratory physiology. Resolution of these gaps in knowledge is limited by the current technology used to measure or infer physiological O_2: Clark electrodes, fibre-optic probes and respirometry chambers. The limitations and issues surrounding these technologies include biological accuracy, *in situ* versus *in vivo* measurements, consumption of the measured analyte and the confounding variable of immobilization.

1.3 Current methods for monitoring O_2 *in vivo*

Measurement of internal PO_2 is essential for a more complete understanding of insect respiration. For example, it has previously been crucial in elucidating gas exchange patterns and hypoxia responses (Greenlee et al., 2013; Groenewald et al., 2012; Matthews and White, 2011b). Likewise, fibre-optic probes and Clark electrodes have been crucial in measuring and inferring internal PO_2, although these methods have several drawbacks and limitations when used in insects.

Clark microelectrodes are platinum electrodes that measure O_2 via reduction of molecular O_2 at the cathode: $O_2 + 4e^- + 2\ H_2O \rightarrow 4\ OH^-$ (Amao, 2003; Severinghaus and Astrup, 1986). Because of their small size (tip diameters of less than 10 μm), these electrodes have been used to measure internal PO_2 in animals as small as bumblebees (Komai, 2001). While useful in measuring PO_2 within small animals, there are several disadvantages to using Clark electrodes. Firstly, Clark electrodes consume O_2 in the process of measuring it, which

is a barrier to accurate measurements – an ideal sensor would not consume the analyte it is measuring (Amao, 2003; Wang and Wolfbeis, 2014). Secondly, Clark electrodes are subject to electrical interference, which can contribute to errors (Amao, 2003). Studies comparing the *in vivo* accuracy of Clark electrodes to fibre-optic probes concluded that fibre-optic probes provide more reliable and more stable measurements (Hopf and Hunt, 1994).

Fibre-optic probes are also able to directly measure internal PO_2, but they are relatively more accurate than Clark electrodes. Direct measurements are achieved by inserting the fibre-optic probe into the insect's trachea or haemocoel, a process that requires the insect to be immobilized (Matthews et al., 2012; Matthews and White, 2011b; Schilman et al., 2008). The stress of an invasive probe and immobilization can increase an insect's metabolic rate, which produces inaccurate measurements (Cutkomp et al., 1976; Kivleniece et al., 2010; Matsumoto et al., 2003). Development of an implantable sensor that can directly monitor internal PO_2 would allow for the pursuit of research questions that would have previously been unanswerable due to the limitations of fibre-optic probes and Clark electrodes.

1.4 Fundamentals of fluorescence and quenching

The implantable sensors developed within this thesis will be based upon the principle of O_2-quenched fluorescence. Fluorescence begins when a photon of excitation light is absorbed by a fluorophore. The absorbed photon excites an electron from an orbital closest to the nucleus (the ground state) to an orbital further away (a higher energy state) (Conchello and Lichtman, 2005; Lakowicz, 2006). After being excited to a higher energy orbital, the electron returns to its ground state by emitting a photon at a lower energy (longer)

wavelength than the one that was absorbed. This phenomenon of a fluorophore emitting light at a longer wavelength than the light it absorbs is referred to as the Stokes shift. A larger stokes shift will result in greater separation between the absorption and emission spectra of a fluorophore. For many applications, an ideal fluorophore has a large stokes shift with a single emission peak. The steps involved in fluorescence can be visualized with a Jablonkski diagram (fig. 1.1).

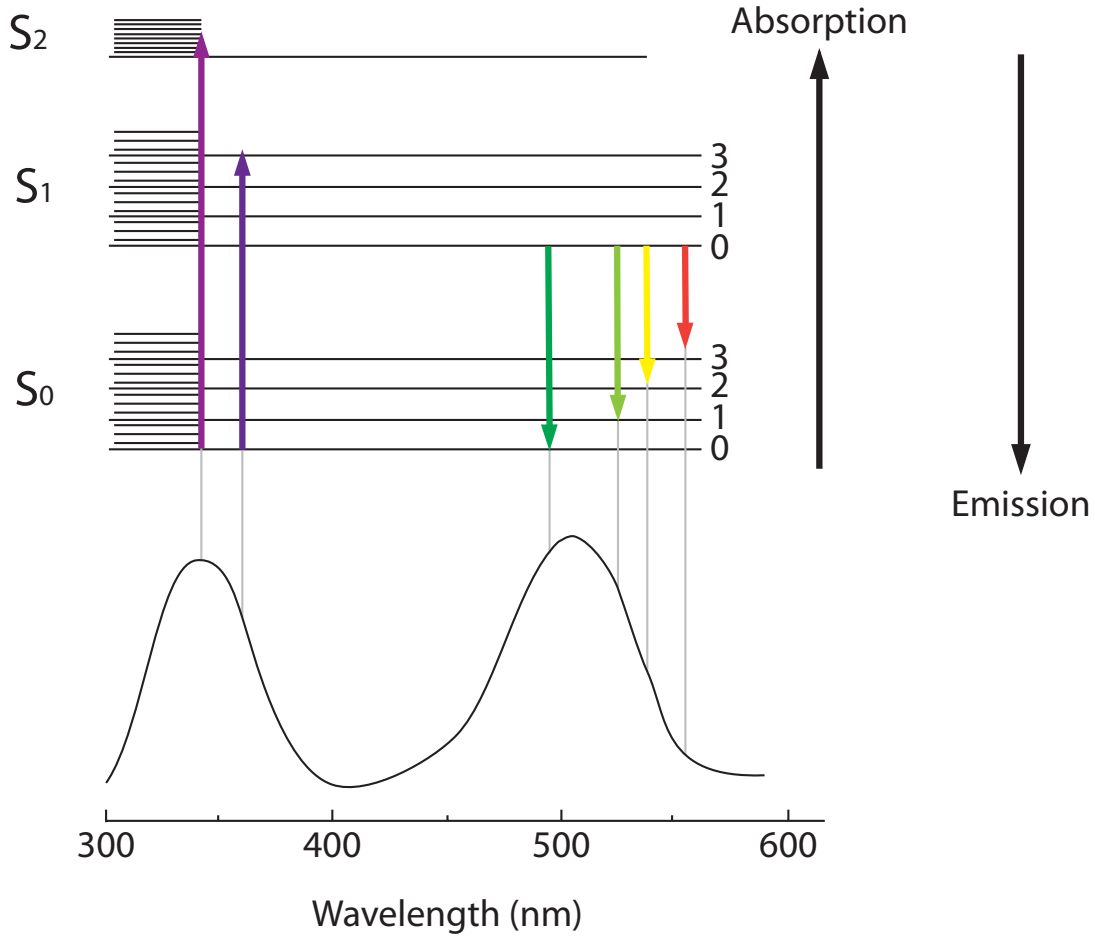

Figure 1.1: A Jablonski diagram illustrating photon absorption (arrows pointing up) with an absorption peak at 350 nm, and photon emission (arrows pointing down) with an emission peak at 500 nm. S_0 indicates the ground state, S_1 indicates the lowest energy orbital, and S_2 indicates the highest energy orbital. Gray lines align the respective arrows with the wavelength of the photon absorbed or emitted (Conchello and Lichtman, 2005).

Many O_2 sensing applications rely on the process of fluorescence quenching, which refers to a decrease in fluorescence intensity in the presence of an analyte. The process of quenching can either be dynamic, also referred to as collisional, or static (Lakowicz, 2006). With static quenching, the analyte combines with the fluorophore in the excited state to form a non-fluorescent complex (Lakowicz, 2006) whereas in dynamic quenching, the analyte (most commonly O_2) collides with the excited fluorophore, absorbs the energy non-radiatively, and returns it to the ground state without the emission of a photon (Lakowicz, 2006). Collisional quenching via O_2 can be explained by the Stern-Volmer relationship:

$$\frac{I_0}{I_f} = 1 + K_{sv} \cdot PO_2$$

Where:

I_0 = Intensity of the dye without the quencher (O_2)

I_f = Intensity of the dye with the quencher

K_{sv} = The Stern-Volmer constant

PO_2 = The partial pressure of O_2 (atm)

Within the Stern-Volmer relationship, all of the fluorescence intensities at each PO_2 concentration are normalized to the fluorescence intensity recorded in the absence of the O_2 quencher (0 atm O_2). At higher PO_2 concentrations the I_f value decreases, resulting in a larger ratio of I_0:I_f. Ideally, there is a linear relationship between I_0:I_f and PO_2, as a linear Stern-Volmer plot indicates that all of the fluorophores are equally accessible to the analyte (Lakowicz, 2006). Temperature will have an effect on the linearity and slope of the relationship due to the nature of collisional quenching. At higher temperatures the diffusion

coefficient of O_2 increases, resulting in more collisions between the fluorophore and O_2 and a greater degree of quenching (Lakowicz, 2006).

Fluorescence quenching is used within fibre-optic probes and will remain essential for an implantable O_2 sensor. The important differences between fibre-optic probes and implantable O_2 sensors lie in the degree of their invasiveness and their ability to deliver spatially specific PO_2 measurements.

1.5 Fluorescent Implantable Elastomer Tags

In recent years, there has been a push to create implantable O_2 sensors as a viable alternative to fibre-optic probes, Clark electrodes and respirometry chambers. Implantable O_2 sensors could allow for the direct measurement of PO_2 within organisms that are too small for fibre-optic probes. They could also provide spatially specific PO_2 measurements and be implanted in multiple locations throughout the body. Furthermore, with an implanted O_2 sensor animals would not have to be tethered during measurements. For implantable O_2 sensors to be used *in vivo*, they must be visible through the cuticle of the insect.

Visualizing fluorescent dyes through insects' integument has already been demonstrated with Visible Implantable Elastomer Tags (VIETs), which are currently used to permanently tag individuals in populations of species that are morphologically indistinguishable, such as fish, crustaceans, earthworms and blowflies (Butt and Lowe, 2007; Moffatt, 2013) allowing for long-term tracking and monitoring. These tags are sold as a liquid polymer containing a fluorescent dye that is excited by ultraviolet light. The polymer is mixed with a curing agent before it is injected into an individual subcutaneously, where it cures into a solid *in vitro* (Dinh et al., 2012). One advantage of VIETs is that they do not

affect the implanted organism's lifespan. For instance, in a study using giant shrimp, no significant difference in mortality was found between individuals implanted with VIETs and non-implanted individuals (Dinh et al., 2012). They have also been implanted into blowfly larvae to test their compatibility across life-stages. Again, no significant difference in mortality or development rate was found between individuals implanted with VIETs and non-implanted individuals (Moffatt, 2013). Because the implantable O_2 sensors I developed in this thesis are inspired by VIETs, I have named them Fluorescent Implantable Elastomer Tags (FIETs).

FIETs are different from VIETs in two ways: the number of dyes used and the implantation process. The first difference between VIETs and FIETs is that the latter contains two dyes rather than one. Previously, *in vivo* O_2 sensors have been developed based on single fluorescence intensity, where a single dye is sensitive to a specific analyte and the analyte's concentration is measured by changes in the dye's fluorescence (Klimant et al., 1999; McDonagh et al., 1998). Measuring an analyte's concentration from a single fluorescence signal can be problematic, as interference from light scattering and chemicals can cause inaccurate measurements (Valledor et al., 2006). Ratiometric dye systems account for interference from light scattering and other factors by using a reference dye in addition to an indicator dye.

With a ratiometric dye system, the fluorescence of the indicator dye changes in the presence of the specified analyte via quenching (Demchenko, 2010; Lakowicz, 2006). However, a reference dye is unaffected by the presence of the same analyte, thus accounting for any variability or interference from the environment (Demchenko, 2010; Xu et al., 2001). For example, if there is variability within the excitation intensity between measurements, it

will affect the intensity of both the reference and the indicator dye (Broder et al., 2007). Taking a ratio of both dyes' intensities will correct for this variability, resulting in an accurate measurement of the analyte (fig. 1.2).

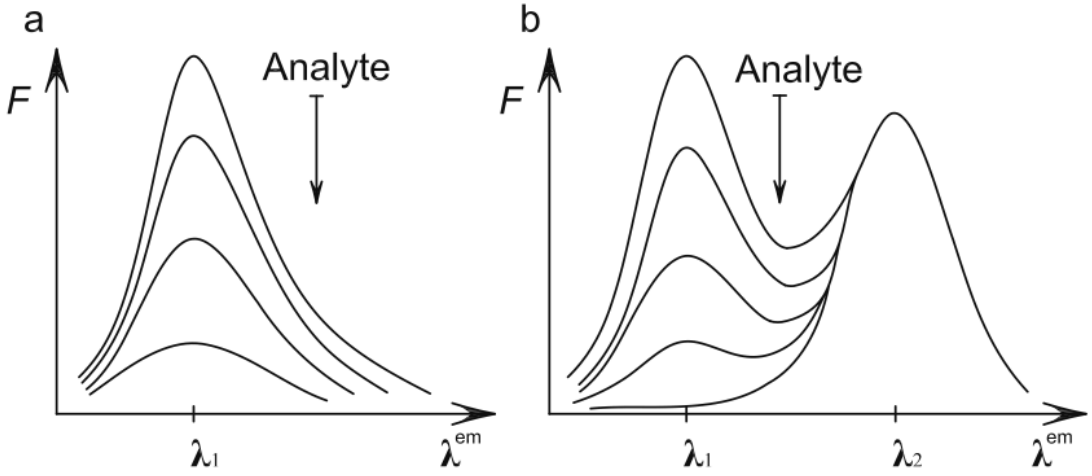

Figure 1.2: Fluorescence of the wavelength emitted by the indicator dye (λ_1) decreases as the concentration of analyte increases (a). The fluorescence of the wavelength emitted by the reference dye (λ_2) is unaffected by the increasing concentration of the analyte (b) (Demchenko, 2010).

The second difference between VIETs and FIETs is that FIETs are cured from liquid droplets into solid microspheres outside of the animal's body. Because the FIETs' purpose is to detect O_2, they must be made of an O_2-permeable material that can be cured from a liquid to a solid. The material commonly chosen for O_2 sensing applications is polydimethylsiloxane (PDMS), which can remain liquid for up to 48 hours before curing into a solid, allowing for sufficient time to form the FIETs (Jiang et al., 2012).

To summarize, the FIETs are composed of a ratiometric dye system suspended within PDMS, this material is broken up into liquid droplets that are then cured into a solid. In order to make the precursor droplets of FIETs, this study will employ methods from the field of microfluidics.

1.6 Microfluidics and implantable elastomer tags

Microfluidics refers to the engineered manipulation of fluids at the microscale, with volumes ranging between 10^{-9} and 10^{-18} litres (Whitesides, 2006). The most common application of microfluidics is the creation of designer emulsions using a microfluidic chip, in which two immiscible liquids are carefully mixed together to create microdroplets (Shah et al., 2008). Simply shaking a container holding the two immiscible liquids can produce an emulsion: a good example of this is shaking a bottle of oil and vinegar to produce salad dressing. However, this example occurs at the macroscale, whereas a microfluidic chip deals with volumes at the microscale. The behavior of fluids at the microscale differs dramatically from that at the macroscale, and it is this difference that allows small volumes of fluid to be precisely manipulated.

One notable characteristic of the microscale is the presence of a laminar flow regime. Laminar flow refers to the condition of a fluid in which the movement of a particle in a fluid stream is not a random function of time, whereas the opposite is true of turbulent flow (Beebe et al., 2002). Turbulent flow refers to chaotic movement of the liquid, such as a fast-moving river with eddies and whirlpools. By contrast, laminar flow is orderly and tends to occur in high viscosity liquids moving at lower velocities through small channels. For instance, honey moving through a straw would have laminar flow. The condition or flow regime of a fluid in a channel is characterized by the Reynolds Number (Re), which is given by the following formula:

$$Re = \frac{\rho v D_h}{\mu}$$

Where ρ is the fluid density, v is the fluid velocity, μ is the fluid viscosity and D_h is the hydraulic diameter of the channel (Beebe et al., 2002). A fluid with a Re below 2300 is more

likely to be characterized as laminar flow, but once the fluid surpasses Re of 2300 it becomes increasingly turbulent (Beebe et al., 2002). The hydraulic diameter of the channel through which a liquid is flowing affects the Re; as the diameter decreases so does the Re of the liquid, resulting in a more laminar flow. Laminar flow is essential for the creation of designer emulsions, as it allows for careful control over droplet size and uniformity.

At the macro-level, two liquids coming into contact with each other will mix convectively. An example of this would be a stream of milk mixing into a cup of coffee (Whitesides, 2006). However, at the microscale two fluid streams will only mix by diffusion (Beebe et al., 2002). Diffusion occurs across the contact surface of the two liquids, increasing as the contact time between the two liquids increases (Beebe et al., 2002). Within designer emulsions, a hydrophobic and hydrophilic liquid come into contact with one another, meaning that neither diffusion nor convective mixing takes place. The lack of convective mixing allows for the creation of dispersed droplets suspended in a continuous phase, the total mixture of these droplets and the continuous phase is known as a uniform emulsion (Beebe et al., 2002; Utada et al., 2005). Within a microfluidic chip, the liquid that composes the droplets is referred to as the disperse phase and the liquid that the droplets are suspended in is referred to as the continuous phase. The disperse phase and the continuous phase are either hydrophilic/hydrophobic (for example, water droplets in oil) or hydrophobic/hydrophilic (fig. 1.3).

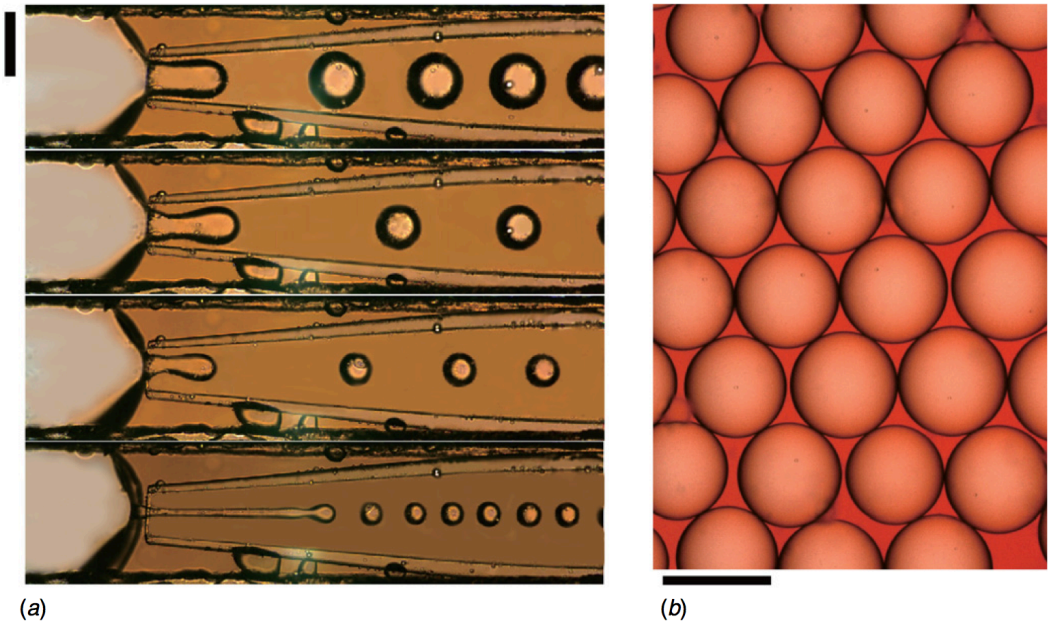

Figure 1.3: (a) Production of dispersed silicone oil droplets (with 0.25% volume per volume Span 80) in a continuous phase of water and glycerin (with 0.25% weight per volume sodium dodecyl sulfate). (b) Photomicrograph of the silicone beads post-production (Jiang et al., 2012).

There are a variety of microfluidic chip designs that may be used to achieve uniform emulsions, ranging from compression-fitting crosses connected to PEEK capillary tubing, to entire complex flow geometries molded from PDMS (Jiang et al., 2012; Shah et al., 2008). However, the microfluidic chip design most accessible to researchers uses only common lab materials and involves the alignment of a pulled glass capillary within a flame polished one. In these chips the disperse phase flows through a microcapillary that has been pulled to have a fine orifice of a specified diameter. This microcapillary is placed inside of a channel containing the continuous phase, which flows in the same direction as the disperse phase. The coaxial flow of the dispersed phase and the continuous phase allows the continuous phase to sweep the dispersed phase off of the microcapillary orifice as it exits, thus facilitating the formation of droplets (Shah et al., 2008). This technique of forming droplets

is termed coaxial flow, or co-flow, referring to the dispersed and continuous phase flowing the in same direction (Shah et al., 2008).

When the dispersed and continuous phases flow at lower velocities in a coaxial flow chip, the droplets will have a larger diameter than that of the capillary orifice and form directly from the orifice in a process known as "dripping" (Shah et al., 2008). If the flow rates of both phases are increased then a jet will begin to form, causing the droplets to decrease in diameter and form further down the channel, in a process known as "jetting" (Shah et al., 2008). In order to achieve jetting, the continuous phase must be several times more viscous than the disperse phase (Utada et al., 2005). It is important to note that jetting has been shown to result in less uniformly sized droplets compared to dripping (Shah et al., 2008; Utada et al., 2005). In general, jetting produces large, non-uniform droplets whereas dripping produces small, uniform droplets (Utada et al., 2005) (fig. 1.4).

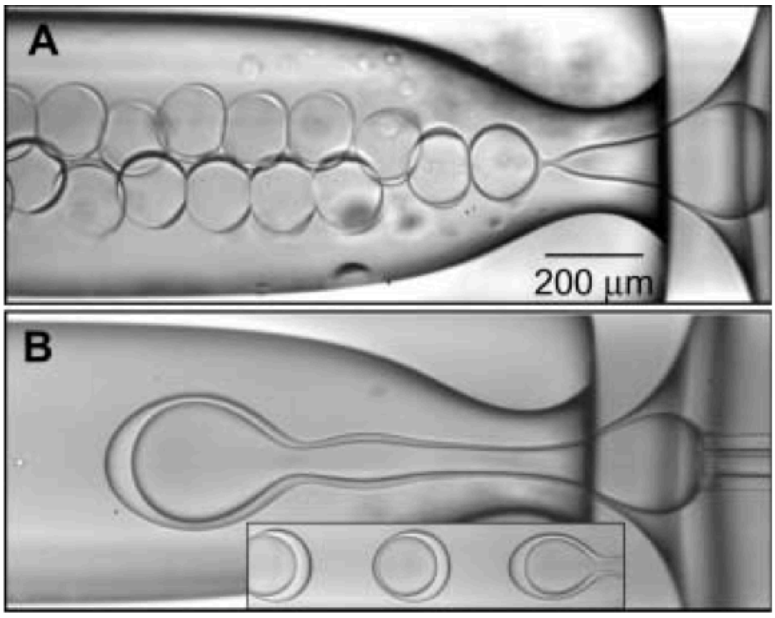

Figure 1.4: Formation of double emulsion droplets using an outer liquid of silicon oil with a viscosity (η) of 0.48 Pa·s, a medium liquid of water-glycerin (η= 0.05 Pa·s) and an inner liquid of silicon oil (η= 0.05 Pa·s). Slow flow rates of the dispersed phase and continuous phase result in droplets being formed immediately from the microcapillary orifice (A). Increased flow rates result in jetting and droplets are formed further downstream (B) (Utada et al., 2005).

Flow rates not only contribute to dripping and jetting, they can also be used to fine-tune droplet size (Utada et al., 2005). Previous research has shown that there is a linear decrease in droplet size with increasing continuous phase flow rate until it becomes more than three times greater than the disperse phase flow rate. At this ratio the flow regime changes from dripping to jetting, resulting in an increase in droplet size (Utada et al., 2005). By adjusting the flow rates and viscosities of the continuous and disperse phases, a wide variety of droplet sizes can be made.

Fine-tuning the droplets within an emulsion to a desired size is a challenging obstacle but the stability of the created emulsions must also be considered. Emulsions are inherently unstable, due to the large area of interface created by the dispersed droplets (Taylor, 1998). This large interface area results in a Gibbs free energy of formation greater than zero, as a

consequence emulsions have a tendency to break down or homogenize (Taylor, 1998). Emulsions may be destroyed in one of two ways, either by Ostwald ripening or by coalescence (Bibette et al., 1999). Ostwald ripening occurs without the rupturing of the interfacial film that contains the dispersed droplets (Bibette et al., 1999; Taylor, 1998). According to the Young-Laplace equation, smaller droplets have a higher internal pressure compared to larger droplets (Beebe et al., 2002). This high pressure causes material from smaller droplets to diffuse through the continuous phase and deposit into larger, lower-pressure droplets (Taylor, 1998). In Ostwald ripening smaller droplets disappear as the average diameter of dispersed droplets increases (Taylor, 1998). While the interfacial film remains intact during Ostwald ripening, the film of the dispersed droplets is ruptured during coalescence (Taylor, 1998). Coalescence also dictates that the droplets must be in close proximity, while the opposite is true of Ostwald ripening (Bremond et al., 2008; Taylor, 1998). During coalescence the droplets come closer together and pressure increases at their contact surface, causing the interfacial film to drain (Bremond et al., 2008). As the interfacial film grows thinner Van der Waals forces interact between the two droplets, hastening the destruction of the interfacial film and the fusion of the droplets (Bremond et al., 2008; Taylor, 1998). In order to create a stable emulsion and prevent Ostwald ripening or coalescence from occurring, a surfactant can be added to both the disperse phase and the continuous phase.

Overall, the microfluidic chip produced must be able to make uniform emulsions of the FIET material within the desired size range. Ideally, the microfluidic chip will exhibit a dripping regime, which provides highly uniform emulsions. The emulsions must also be sufficiently stable to allow time for the FIET precursor droplets to cure into solid

microspheres, therefore finding a biocompatible surfactant to stabilize the emulsions will be important.

1.7 Thesis goals

The goal of my thesis is to produce implantable O_2 sensors (FIETs) as an alternative to fibre-optic probes for use within insects and other small animals. The FIETs will be able to provide spatially specific information about internal PO_2 and allow for multiple measurements of PO_2 to be taken simultaneously. I have previously outlined research questions that these FIETs could be used to address, such as the effectiveness of O_2 guarding within dampwood termites, whether O_2 diffusion distance is a constraint on insect body size and elucidating the respiratory mechanisms of the phantom midge.

The ideal size of these FIETs is 70 μm or less, so that they are implantable and minimally invasive. The matrix of the FIETs will be PDMS, as it is permeable to oxygen and has been used previously in O_2 sensing applications (Jiang et al., 2012). Suspended within the FIETs' PDMS matrix will be a ratiometric dye system, which will not only provide accurate measurements of PO_2 but also account for any scattering or interference. The first step to making FIETs is to develop a microfluidic chip capable of making uniform emulsions with droplets smaller than 70 μm. Therefore, I will begin by laying out the steps taken to develop a microfluidic chip and evaluating the uniformity of the emulsions produced. Next, I will discuss how the FIETs were designed, assess their photostability and demonstrate their use in detecting PO_2 within an autofluorescent system.

2: Research chapter

2.1 Introduction

Two parameters of fluorescent implantable elastomer tags (FIETs) need to be identical within batches in order to ensure accurate measurements: O_2 response and diameter. A reliable microfluidic chip design contributes to uniform size distribution within batches of FIETs, while a robust ratiometric dye system ensures a consistent response to changing oxygen concentrations. Even if the utmost care is taken in both of these regards, there are other confounding factors, such as photodegradation and autofluorescence, which may affect the performance of the FIETs. Accounting for these factors in the FIETs will allow for a more accurate measurement of O_2.

The first step of my research project was to create a functional microfluidic chip to produce uniform emulsions of FIETs. There are two styles of microfluidic chips appropriate for FIET production: either a T-junction chip or a glass capillary chip (Jiang et al., 2012; Shah et al., 2008). Flow focusing (when the continuous phase flows perpendicular to the disperse phase) is used to produce droplets within a T-junction chip, whereas coaxial flow (both phases flow in the same direction) is employed within a glass capillary chip.

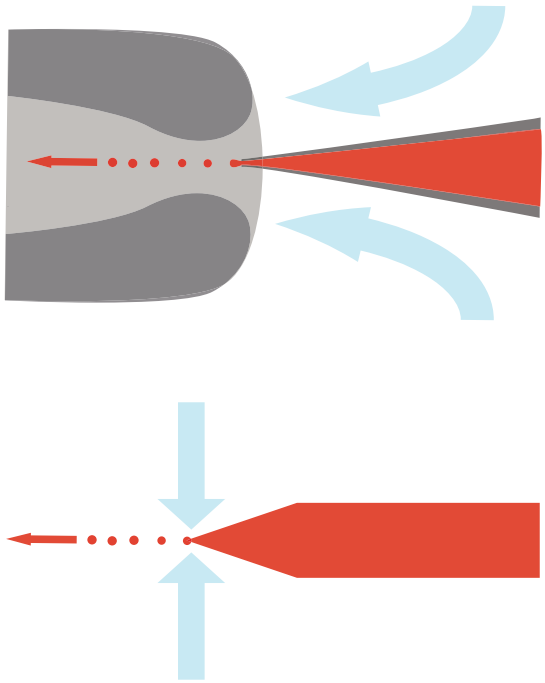

Figure 2.1: Coaxial flow (top) versus flow-focusing (bottom) design in microfluidic chip. Red indicates disperse phase and blue indicates continuous phase. Within coaxial flow the grey indicates a flame-polished glass capillary and a pulled glass capillary.

A T-junction chip consists of micro-channels arranged perpendicularly to one another (Jiang et al., 2012), while the glass capillary chip consists of a pulled microcapillary (also known as the injection tube) aligned within a collection tube (Utada et al., 2005). One advantage of a T-junction chip is that it is composed entirely of either polymethylmethacrylate (PMMA) or PDMS. Using one material means that the base and lid can be fused together (with heat for PMMA and plasma treatment for PDMS) to form a water-tight bond (Jiang et al., 2012). Heat or plasma bonding are not possible with glass microcapillary chips because they contain a mixture of materials (glass and PMMA), therefore both two-part epoxy and solvent-based cement must be used instead (Er Qiang et al., 2014; Utada et al., 2005). While heat and plasma bonding ensure a stronger bond than cement, the T-junction chip is only feasible for researchers with a computer numerical

control (CNC) router with micro end mills (Jiang et al., 2012). For this reason, I chose a glass microcapillary design in order to manufacture the O_2 FIETs. Within the glass microcapillary design, control over the size of the FIETs is limited by the diameter of the exit orifice of the injection tip and by the viscosity of the continuous phase (Shah et al., 2008; Utada et al., 2005). Furthermore, there may be discrepancies between batches of FIETs because the injection tube and collection tube are aligned by hand. While the difference in alignment between the injection and collection tube may be slight, at the micro-scale this can result in a vastly different flow regime (Beebe et al., 2002). However, size consistency is more important within batches than between, and consistency in FIET PO_2 response surpasses both of these concerns.

Ensuring a consistent PO_2 response by the FIETs also entails choosing an appropriate polymer matrix and ratiometric dye system. I chose PDMS as the matrix because of its high permeability to O_2 (Jiang et al., 2012) and its biocompatibility (Bélanger and Marois, 2001; Peterson et al., 2005). My indicator and reference dyes were selected based on several criteria: photostability, excitation and emission wavelengths, dispersion, hydrophobicity, and O_2 sensitivity. The more photostable the dyes, the better, as this allows for accurate measurements of PO_2 over a longer period of time. Both dyes must be excited by the same wavelength of light (within my setup this is 390 nm), and have distinct emission wavelengths with minimal overlap. In addition, both dyes must be hydrophobic to prevent them leaching from the FIETs into an aqueous environment. Lastly, the indicator dye's fluorescence must be quenched in the presence of O_2 whereas the reference dye's fluorescence must remain unchanged.

I selected platinum (II) meso-tetra(pentafluorphenyl)porphine (PtTFPP) for the indicator dye as it meets all of the aforementioned criteria. PtTFPP is hydrophobic, it disperses homogenously into the PDMS matrix, it has an emission peak at 650 nm and is excited by 390 nm light (Jiang et al., 2012). Most importantly, the fluorescence of PtTFPP is quenched in the presence of O_2. Previous studies have shown a linear relationship between PtFPPP fluorescence and PO_2 by using a Stern-Volmer plot (Cao et al., 2004; Jiang et al., 2012). Furthermore, fluorinated metalloporphyrins, such as PtTFPP, are more resistant to photo-oxidation than their non-fluorinated counterparts, and are suitable for measuring low levels of O_2 (Wolfbeis, 2005).

For the reference dye, I chose a hydrophobic organic light emitting diode (OLED) polymer, poly(9,9-dioctylfluorene-*alt*-benzothiadiazole) (F8BT). This OLED is excited by the same wavelength of light as PtTFPP, but has an emission peak at 550 nm. Compared to other OLED polymers, F8BT is relatively resistant to photo-oxidation (Brenner et al., 2015) and has minimal aggregation within the PDMS matrix. While these dyes may meet the initial criteria of the ratiometric dye system, several other factors need to be considered to ensure the accurate measurement of O_2.

The most important factor to consider is the rate and magnitude of photobleaching (the reduction of emission intensity in a fluorophore following repeated illumination) for both the indicator dye and the reference dye within the FIETs. Fibre-optic probes rely on luminescence lifetimes, rather than fluorescence intensity, to measure PO_2. As a result, their measurements are independent of photobleaching, which is a clear advantage over applications that rely on fluorescence intensity (Wolfbeis, 2005). The FIETs in this thesis rely on the intensity of the reference dye and the indicator dye to measure PO_2. Therefore,

any photobleaching must be corrected for when taking measurements. Without a correction, significant photobleaching of the dyes could result in an inaccurate measurement of PO_2. While photobleaching is the most significant barrier to accurate measurements of PO_2, there are other potential confounding factors, such as temperature, pH and the inner filter effect, that should also be investigated (Wolfbeis, 2005). Most importantly, the FIETs must be able to overcome the confounding effect of autofluorescence.

Autofluorescence refers to the natural fluorescence of biological compounds, such as mitochondria and proteins. This can be advantageous in some applications that seek the localization of a particular protein (Lakowicz, 2006), but it can also interfere with measurements (Cao et al., 2004; Koga et al., 2009). Autofluorescence is observed in virtually all biological imaging applications in which ultraviolet or blue light is used to excite a fluorophore. Strong autofluorescence is frequently seen in insect cuticles, skeletal muscles and organs (Klaus et al., 2003). Several studies have investigated how to quench or mitigate autofluorescence (Koga et al., 2009), and knowing how to measure PO_2 with the FIETs in an autofluorescent system will be vital in moving towards *in vivo* measurements. Agar can be used as a biologically relevant medium to simulate the FIETs' performance in an insect because it is permeable to O_2, transparent, and exhibits autofluorescence.

With a functional microfluidic chip and a robust ratiometric dye system, I can ensure the production of uniformly sized FIETs that produce accurate measurements of PO_2. Ideally, these FIETs will have a uniform size distribution around 70 μm or less in diameter, which will minimize trauma during and after implantation. Most importantly, the FIETs must exhibit a linear fluorescent response when exposed to increasing PO_2 and be photostable enough to acquire meaningful data. Furthermore, the FIETs must be able to operate within an

autofluorescent system *in situ* before being considered for *in vivo* applications. If the FIETs meet these specifications then they could potentially be used to address currently unanswered questions within the field of insect respiratory physiology.

2.2 Materials and methods

2.2.1 Construction of the microfluidic chip

Construction of the microfluidic chip began with the base and lid, which were composed of polymethylmethacrylate (PMMA) pieces measuring 50 mm × 15 mm × 10 mm and 50 mm× 15 mm × 4 mm respectively. A 1.3 mm × 1.3 mm channel was milled lengthwise through the chip base using a Nomad 883 computer number controlled (CNC) machine (Carbide 3D, Torrance, CA, USA); two holes, 1.5 mm in diameter each, were drilled into the center of the lid at 25 mm and 45 mm and aligned with the channel in the base. Following this, both the base and the lid were cleaned sequentially with filtered ethanol, distilled deionized water and compressed air. The base and lid were then welded together using a solvent-based cement (Weld-On 4, IPS Corporation, Compton, CA, USA) and clamped for 30 minutes until the epoxy had completely evaporated. The channel was then re-cleaned with several streams of filtered ethanol, distilled deionized water and compressed air.

Standard type 1B120-4 borosilicate glass capillaries (World Precision Instruments, Sarasota, FL, USA), measuring 4 mm in length, 1.2 mm OD, 0.68 mm ID, were cleaned in the same manner as the chip base and lid in order to form the injection tube and the collection tube. To make the injection tube, the first glass capillary was placed in a Model P-97 micropipette puller (Sutter Instrument, Novato, CA, USA) and pulled to have a final tip

diameter of 13 μm. This injection tube was then inserted into the channel and fixed into place using two-part epoxy (Elmer's Products Inc., High Point, NC, USA). The injection tube was rotated within the channel immediately following epoxy application in order to create an effective seal. Using a micro-jet torch (Pro-Iroda Industries, Cleveland, OH, USA), I flame polished the end of the second glass microcapillary until the orifice was roughly half of its original size to form the collection tube. With the aid of an SZX10 dissection scope (Olympus Canada Inc., Richmond Hill, ONT, Canada), this collection tube was aligned with the tip of the injection tube and fixed into place with two-part epoxy. For the inlet of the disperse phase, a section of 22-gage hypodermic tubing was epoxied to a section of polytetrafluoroethylene (PTFE) tubing. This inlet was then cleaned with filtered ethanol and compressed air to remove any metal filings. For the continuous phase inlet, a section of PTFE tubing cleaned with filtered air was epoxied to the second hole in the chip lid. A schematic of the microfluidic chip is shown in figure 2.2.

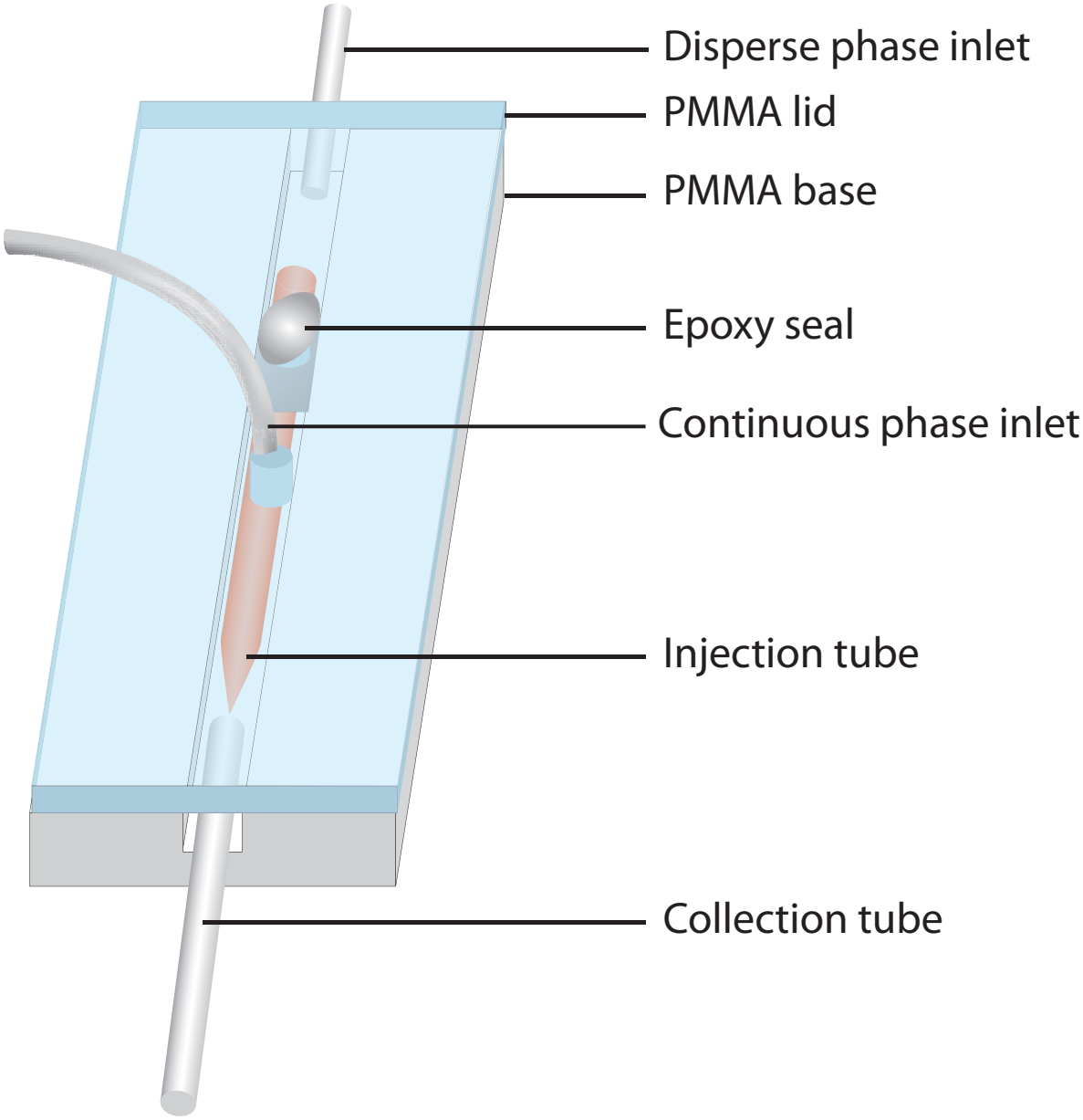

Figure 2.2: A schematic of the microfluidic chip and its components after being assembled.

2.2.2 Operation of the microfluidic chip and uniformity

Previous research has shown that impurities within liquid phases can clog the injection tip (Jia Ming et al., 2014). Therefore, the continuous and disperse phases were filtered as they entered the chip using syringe-adaptable filters with a 0.45 μm pore size (MilliporeSigma, Etiobicoke, ONT, Canada). The flow rates of the disperse phase and

continuous phase were controlled using two PHD Ultra precision syringe pumps (Harvard Apparatus, Holliston, MA, USA).

To evaluate the uniformity of the emulsions produced by the microfluidic chip, Sylgard 184 PDMS (Dow Corning Corporation, Auburn, MI, USA) without the ratiometric dye system was used. A 1:1 volume ratio of PDMS curing agent:base was used as the disperse phase. The prescribed ratio of curing agent:base is 1:10, but this produced a highly viscous mixture which was difficult to form into droplets. Previous research has successfully used a 4:6 weight ratio of curing agent:base, so I adjusted the ratio within my own microfluidic set up (Jiang et al., 2012). To see whether a more viscous continuous phase would yield a more uniform emulsion in the chip, I made a comparison between 1% (w/v) sodium dodecyl sulfate (SDS) and 5% (w/v) Kolliphor P 188 (Sigma Aldrich, Oakville, ONT, Canada) in distilled deionized water. The continuous and disperse phase flow rates were varied and the diameters of the resultant FIETs were measured to evaluate the size range and uniformity of FIETs produced. The disperse flow rates used were 1 μL/min, 0.5 μL/min and 0.25 μL/min. At each of these disperse phase flow rates the continuous phase flow rate was varied from 100 μL/min, 200 μL/min, 300 μL/min and 500 μL/min. Time was allotted between each continuous flow rate change to allow the flow regime within the microfluidic chip to stabilize. The FIETs produced at each combination of disperse phase and continuous phase flow rates were collected and allowed to cure at 25°C. 1 mL of FIETs suspended in distilled deionized water with surfactant (either 5% Kolliphor or 1% SDS) was placed on a glass slide and excess water was wicked away. The prepared FIETs were then imaged using an Orca-Flash 40 LT digital camera (Hamamatsu Photonics K.K, Hamamatsu City, Shizuoka, Japan) attached to an IX73 inverted microscope (Olympus Canada Inc.,

Richmond Hill, ONT, Canada). CellSens software (Olympus Canada Inc., Richmond Hill, ONT, Canada) was used to image and measure randomly selected FIETs. Following measurement of the FIETs, a dispersity index (Đ) was calculated for the emulsions at each combination of flow rate using the following formula:

$$Đ = \frac{standard\ deviation}{mean\ FIET\ diameter} \times 100\%$$

Within the field of emulsion microfluidics, a Đ of less than 3% indicates a highly uniform emulsion (Jiang et al., 2012).

2.2.3 Designing the FIETs

With a functional microfluidic chip in place, I could now focus my attention on the ratiometric dye system within the FIETs. Choosing an indicator dye was straightforward; PtTFPP was selected as it had previously been used in O_2 sensing applications, particularly within polymer-based microspheres (Cao et al., 2004; Jiang et al., 2012). This dye disperses homogenously within the PDMS matrix (as seen in figure 2.7) and has a high quantum yield. However, finding a reference dye for this project that met all of my requirements proved to be difficult.

Table 2.1: Requirements of the reference dye and the indicator dye for the ratiometric dye system within the FIETs

Parameter	Indicator dye	Reference dye
Excitation peak (nm)	390 nm	390 nm
Emission peak (nm)	~650 nm	~530 nm
Response to PO_2	Fluorescence is quenched	Fluorescence is unchanged
Dispersion within PDMS	Homogeneous	Homogeneous
Polarity	Non-polar	Non-polar

At the beginning of this project, I had hoped to use quantum dots as the reference dye. Quantum dots are an appealing reference dye because they have high quantum yield, are resistant to photo oxidation, and are hydrophobic. Unfortunately, quantum dots show extreme aggregation within PDMS, to the point where I could not guarantee a homogenous distribution of them within or between FIETs. Even after extended periods of sonication within the PDMS base (1 hour of accumulated sonication in 2 minute bursts), and experimenting with different solvents (chloroform and toluene), the aggregation persisted. Furthermore, the quantum dots I used were copper-indium/zinc-sulfur (CuI/ZnS), the zinc-sulfur cap of the quantum dots contributes to their photo stability (Kansal et al., 2007), but sulfur is a known inhibitor of the platinum-based PDMS catalyst (Chambon and Winter, 1985; Kloter et al., 2004). As a result, not only did the FIETs have an uneven distribution of reference dye, they were also completely un-curable.

In a bid to find a suitable reference dye, I tried the following candidates: coumarin-6, 7-4-trifluorocoumarin, terbium sulfate, and F8BT. All of these fit the specifications of excitation wavelength (~390 nm) and emission wavelength (~550 nm), but each had their own shortcomings. Coumarin-6 and 7-4-trifluorocoumarin were brilliantly fluorescent and

dispersed homogenously into the PDMS upon first inspection, but photobleached so quickly that no meaningful measurements would be possible using them. Terbium-sulfate also showed bright fluorescence, but exhibited even worse aggregation than the quantum dots. Moreover, terbium-sulfate contains a significant proportion of sulfur, which raised concerns about curing. While F8BT also exhibited aggregation, it was minimal enough that a relatively equal amount of reference dye (and fluorescence) was observed between FIETs of the same size. Because F8BT fit all of the specifications of the reference dye (excited by 390 nm light, emits light at 530 nm, photostable, minimal aggregation, no quenching by O_2, minimal overlap with PtTFPP emission peak) it was chosen as the reference dye. The PtTFPP used in the FIETs was purchased from Frontier Scientific, Newark, USA. The F8BT was purchased from Sigma Aldrich, Saint Louis, USA.

To add the ratiometric dye system to the FIETs, the PtTFPP was dissolved in toluene (concentration of 1 mg mL^{-1}), sonicated for 10 seconds and added to the PDMS base for a final concentration of 0.05 mass percent (the ratio of the mass of the PtTFPP to the mass of the total mixture), the toluene was evaporated off using a vacuum centrifuge (Eppendorf Vacufuge Concentrator, Eppendorf Canada, Missisauga, ONT, Canada). This process was then repeated with F8BT, which was added to the PDMS base for a final concentration of 0.009 mass percent. The emission spectra of the ratiometric dye system can be seen in figure 2.3.

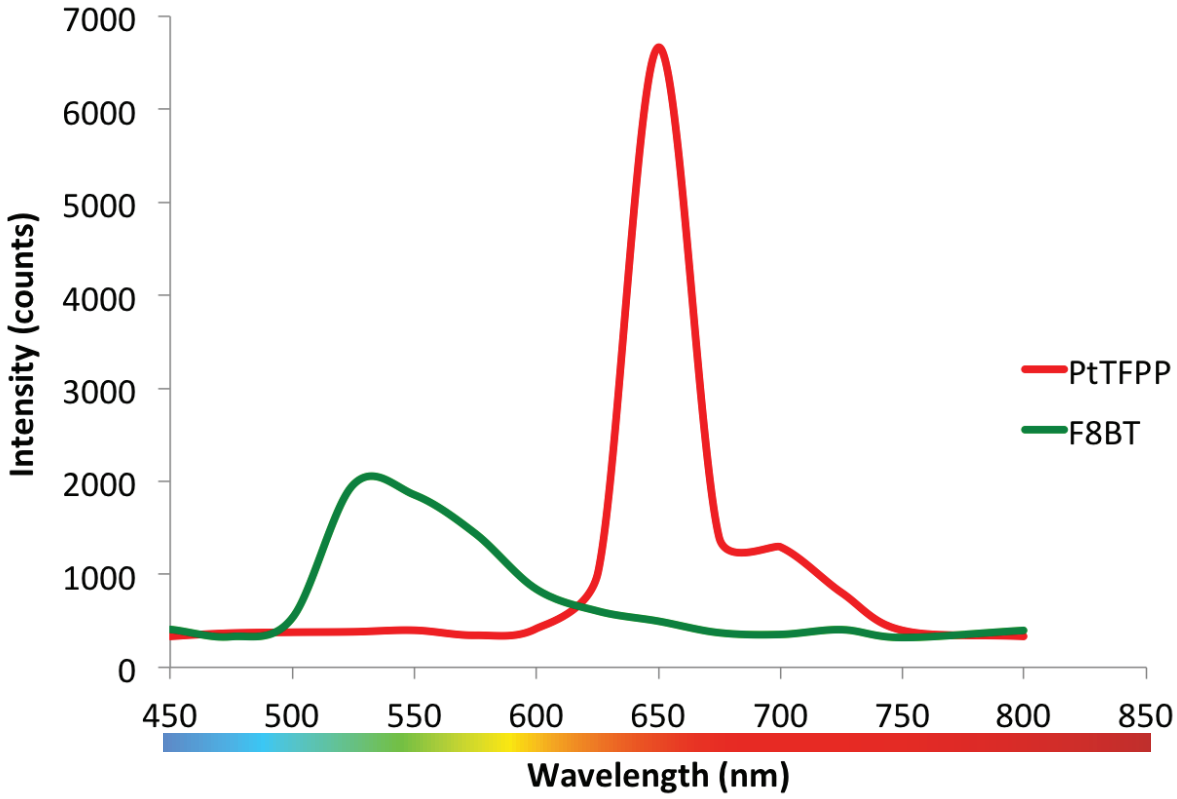

Figure 2.3: A spectrum of the emission peaks of the reference (F8BT) and indicator (PtTFPP) dyes of the ratiometric dye system within the FIETs, taken with an Ocean Optics Flame mini spectrophotometer at 0.21 atmospheres (atm) oxygen.

After the ratiometric dye system was added, the PDMS was mixed in a 7:3 ratio of base to curing agent in order to form the FIET matrix. This ratio of base to curing agent differs from the one used to evaluate uniformity of the microfluidic chip because I observed improved curing and rigidity with a 7:3 ratio compared to a 1:1 ratio. Following production, the FIETs were given 48 hours to cure in the dark at room temperature (19-22 °C).

2.2.4 Response to PO_2

The FIETs were characterized for their sensitivity to O_2 and susceptibility to photobleaching. To characterize the FIET's response to PO_2, a custom imaging chamber for

the IX73 inverted microscope stage was designed using SketchUp software (Trimble Canada, Vancouver, BC, Canada) and then printed from acronitrile butadiene styrene (ABS) plastic using an Ultimaker^2 3D printer (Ultimaker, Cambridge, MA, USA). The inside of the imaging chamber was spray painted black to prevent light scattering within the chamber. Gas inlet and outlet ports were mounted on opposite sides of the chamber to allow the FIETs to be exposed continuously to custom gas mixtures. A schematic and details of the imaging chamber can be found within appendix A of this thesis (fig. A1).

The relationship between PO_2 and FIET fluorescence was established by exposing the FIETs to increasing partial pressures of O_2. The FIETs were placed on a Whatman paper filter (GE Healthcare Life Sciences, Mississauga, ONT, Canada) dried and rinsed of surfactant (using distilled deionized water) via vacuum filtration and then placed on a glass slide. This glass slide was fitted inside of the imaging chamber on the IX73 inverted microscope, and the FIETs were exposed sequentially to custom gas mixtures with PO_2s ranging from 0 to 0.2 atm in 0.02 steps. Custom mixtures of high purity O_2 in a balance of N_2 were produced by metering gas from compressed cylinders (Praxair, Vancouver, BC, Canada) through two mass flow controllers (Alicat Scientific, Tucson, AZ, USA). A 0-100 mL min^{-1} mass flow controller was used to regulate O_2 and 0-500 mL min^{-1} mass flow controller was used for N_2. The mass flow controllers were connected to a USB multi drop box (Alicat Scientific, Tucson, AZ, USA) and Flow Vision MX Gas Mixing software (Alicat Scientific, Tucson, AZ, USA) was used to control the flow rates of both controllers. The gas mixture was humidified to 100 % relative humidity (RH) by first bubbling it through an air-stone submerged in a 500 ml Schott bottle filled with distilled deionized water. Humidified gas mixtures were set to flow continuously over the FIETs at a constant rate of 500 mL min^{-1}.

At each PO_2 the FIETS were exposed to 390 nm light set to 40% intensity from an X-Cite 120 LED light source (Excelitas Canada Inc., Vaudreuil-Dorion, QUE, Canada) and a picture was taken with the Orca-Flash 4.0 LT digital camera using an integration time of 25.05 ms. The emission wavelengths of the indicator dye and reference dye were split using a W-View Gemini image splitter (Hamamatsu Photonics K.K, Hamamatsu City, Shizuoka, Japan) containing long-pass and short-pass wavelength filters. Three minutes of equilibration time was given between measurements to ensure that the gas mixture had fully diffused through the PDMS matrix of the FIETs. To validate the PO_2 within gas mixtures, a fibre-optic flow-through O_2 sensor was placed at the outflow port of the gas chamber and connected to a Microx 4 trace fibre-optic oxygen transmitter (PreSens Precision Sensing GmbH, Regensburg, Germany) (fig. 2.4).

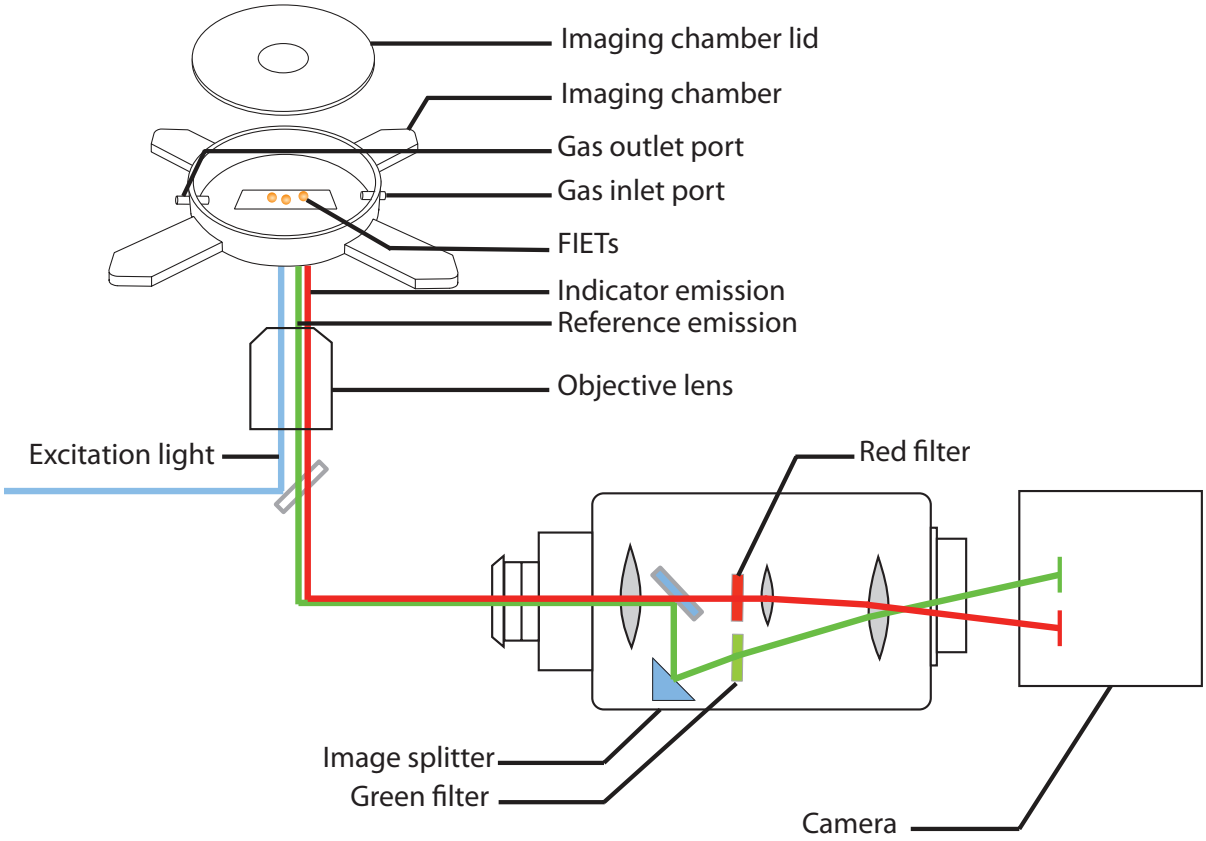

Figure 2.4: Schematic of the imaging chamber on the inverted fluorescence microscope with the emission wavelengths of the ratiometric dye system in FIETs being separated by an image splitter.

2.2.5 Photodegradation and drift in PO_2 measurements

Photobleaching was determined by continuously illuminating three, separate subsets of FIETs from the same batch with 390 nm light from the X-Cite 120 LED light source set at 40% intensity over a ten-minute time period. The FIET subset was placed on a glass slide within the imaging chamber and images were taken with the Orca-Flash 4.0 LT digital camera every ten seconds during the first two minutes of illumination and every one minute afterwards (camera exposure time was 25.05 ms). This protocol was repeated with 0, 0.1 and 0.2 atm PO_2 gas mixtures flowing over the FIETs. Gas mixtures were made and humidified following the same method used to calibrate the FIETs. To ensure the FIETs were exposed to

steady-state PO_2 conditions, all gas mixtures were monitored at the gas outflow port with the fibre-optic O_2 sensor.

2.2.6 Measuring PO_2 *in situ*

Biological systems exhibit autofluorescence that could interfere with the FIETs' measurements. Before implanting the FIETs into an animal, I needed to determine whether they could measure PO_2 in an autofluorescent system.

The FIETs used to measure PO_2 within an agar gel (Fisher Scientific, Fair Lawn, NJ, USA) were made by vortexing the FIET material (7:3 ratio of Sylgard 184 base:curing agent containing 0.05% PtTFPP and 0.009% F8BT) within 10% (w/v) Kolliphor in distilled deionized water. A calibration curve was made for these FIETs using the same method as described in section 2.2.5, except that the FIETs were only exposed to 0, 0.1 and 0.2 atm PO_2.

To create an O_2 gradient within the agar gel, I needed to flush either side of the gel with N_2 gas (0 atm PO_2) and air (0.21 atm PO_2) and force the gases to diffuse through the gel. A chamber was printed from ABS plastic using an Ultimaker^2 3D printer, this chamber was designed to fit on a standard glass microscopic slide, the chamber's dimensions were 35 mm × 35 mm × 10 mm. Within the chamber were three compartments, the middle was filled with 0.5% (w/v) agar containing the FIETs, the second compartment was flushed with humidified, high purity N_2 gas from a compressed gas cylinder, and the third compartment was flushed with humidified room air. Both gases were held at constant flow rates of 15 mL min^{-1}. The agar gel compartment was situated between the N_2 compartment and the air compartment so that each gas could flow on either side of the agar gel (fig. 2.5).

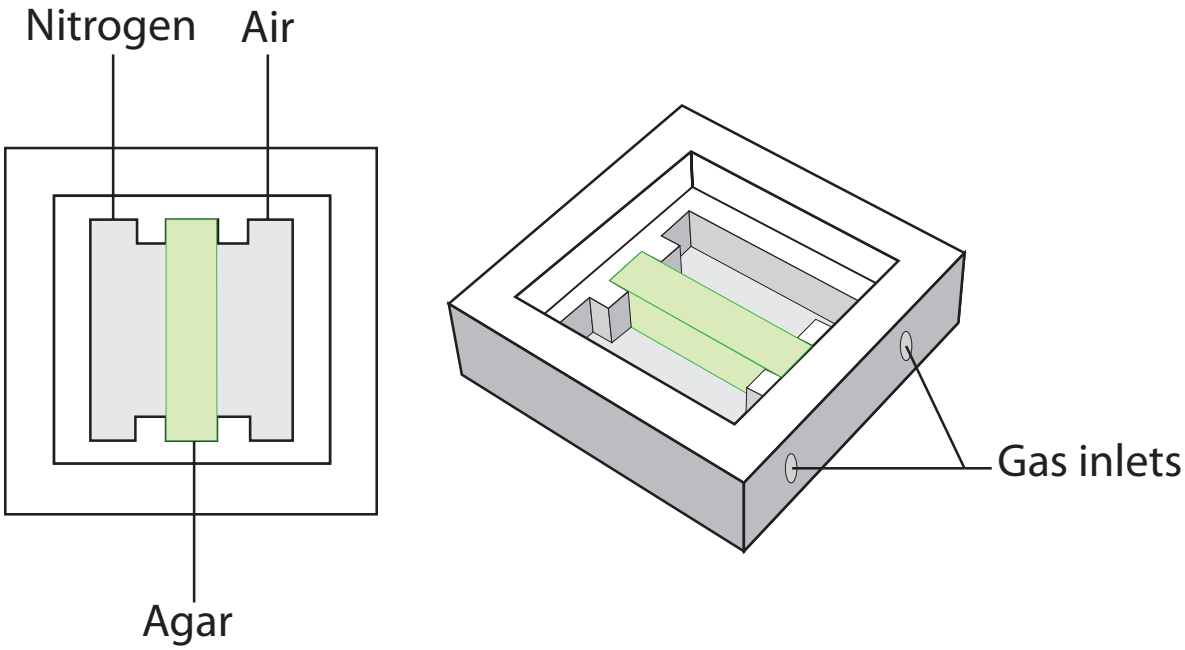

Figure 2.5: Schematic of the chamber used to create an oxygen gradient within a 0.5% agar gel (indicated in green), the chamber measurements are 35 mm × 35 mm × 10 mm.

Using two-part epoxy, the chamber was mounted onto a standard 75 mm × 25 mm glass microscope slide and allowed to cure. The gas inlets were blocked using adhesive putty and a solution of 0.5% (w/v) agar in distilled deionized water was filled to the first lip of the chamber (5 mm in height). After the agar had set, the middle portion of the gel was cut out using a scalpel blade, leaving agar within the N_2 and air compartments. The FIETs were vacuum-filtered and dried on a Whatman paper filter. Using a 22-gage needle, FIETs were randomly scattered on the glass surface within the middle agar compartment. Agar solution was poured over the FIETs within the agar compartment and the compartment was filled up to the first lip. A glass coverslip was placed on top of the liquid agar, while ensuring that there were no bubbles between the agar and the coverslip, before allowing it to set for one hour. After the agar was set, the coverslip was removed and the agar filling the N_2 and air compartments was removed using a scalpel blade, leaving a 22 mm × 7 mm × 5 mm block of

agar containing FIETs dividing the chamber. The adhesive putty blocking the gas inlets was also removed at this time. 100% petroleum jelly (Unilever, Rotterdam, Netherlands) was then spread around the first lip of the chamber and a new coverslip was placed onto the surface of the agar and gently pressed into jelly. Adhesive putty was gently pressed around the edge of the coverslip and along the inside of the chamber to create a seal.

The chamber was then placed on the specimen stage of the IX73 inverted microscope before setting up the O_2 gradient. The N_2 gas flow was controlled using a 0-500 mL min^{-1} mass flow controller, while the air gas flow was controlled with a 0-100 mL min^{-1} mass flow controller. Each gas was hydrated to 100% RH by passing it through an air stone submerged within a 500 ml Schott bottle of distilled deionized water. The N_2 and air entered their respective compartments within the chamber through a length of PTFE tubing that fit loosely within each gas inlet hole. The gap around the PTFE tubing allowing the gas to flow out from the chamber, thus preventing the gas pressure from building up and potentially popping off the cover slip or distorting the agar block. Both gases entered the chamber at a constant flow rate of 15 mL min^{-1}.

The glass coverslip placed over the agar gel prevented the gases from mixing with one another, meaning that diffusion would take place through the agar gel and create an O_2 gradient. I allowed 20 hours of continuous gas flow for the gradient to form. FIETs were randomly imaged along the width of the agar before and after the O_2 gradient was established (Time 0 and Time 1, respectively). FIETs were excited with 390 nm light set to 40% intensity from the X-Cite 120 LED light source and imaged using the Orca-Flash 40 LT digital camera with an integration time of 25.05 ms. Fluorescence intensities were extracted using ImageJ software (see section 2.2.7).

2.2.7 Data analysis

ImageJ software (Schneider et al., 2012) was used to quantify the fluorescence intensity of both the indicator and reference dye. For the calibration curves and photodegradation experiments (fig. 2.9 to fig. 2.14) the background fluorescence was accounted for. Using the oval selection tool, the area of the FIET was fit by hand and the integrated density was measured. The integrated density refers to the mean gray value of a measurement multiplied by the area of the object being measured. After this, three background points surrounding the FIET were randomly selected and their integration density was also measured. The fluorescence intensity of both the indicator and the reference was calculated as corrected fluorescence, where the average integrated density of the background measurements is subtracted from the integrated density of the fluorophore within the FIET.

No background measurements were taken for the calibration curve used to calculate PO_2 within the agar gel and the agar PO_2 measurements themselves (fig 2.15 and 2.16). Instead, the uncorrected integration density of the indicator fluorescence and the reference fluorescence with the FIETs was used as a proxy for fluorescence intensity.

All linear models and statistical tests were carried out using R software (R Development Core Team, 2010).

2.3 Results

2.3.1 FIET uniformity

The size range and uniformity of FIETs produced by the microfluidic chip (using either 1% SDS or 5% Kolliphor as the continuous phase) was evaluated by varying the

continuous flow rate (100, 200, 300 and 500 µl·min^{-1}) and the disperse flow rate (1, 0.5 and 0.25 µl·min^{-1}) in three individual chips for each surfactant. For both surfactants, Đ was calculated at each combination of flow rates and the cumulative relative frequency of Đ within all three microfluidic chips was taken.

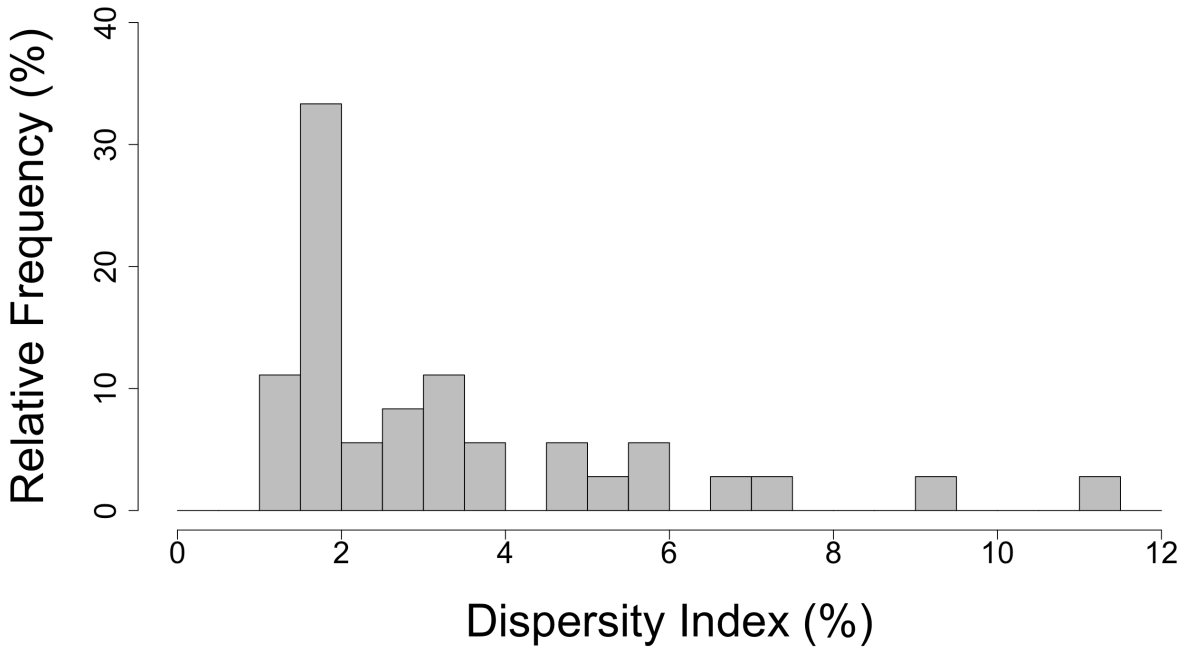

Figure 2.6: The dispersity index measured for each combination of disperse flow rate and continuous flow rate in three microfluidic chips, where the continuous phase is 5% Kolliphor and the disperse phase is 550 cSt Sylgard 184 PDMS (1:1 volume ratio of base to curing agent).

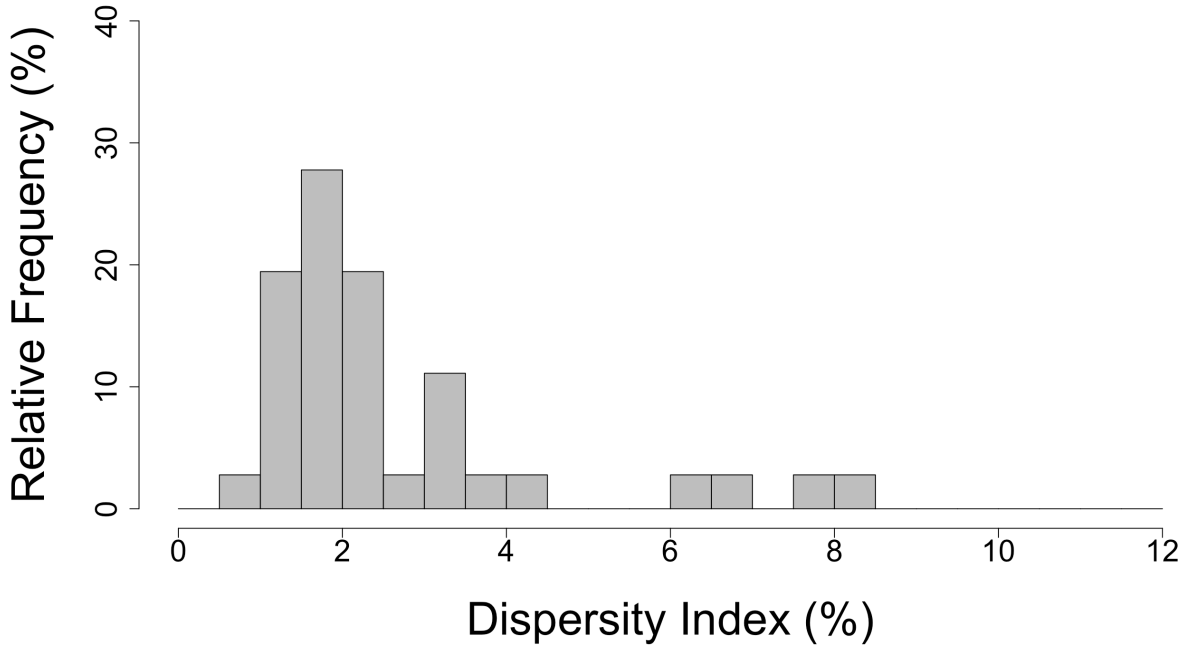

Figure 2.7: The dispersity index measured for each combination of disperse flow rate and continuous flow rate in three microfluidic chips, where the continuous phase is 1% sodium dodecyl sulfate and the disperse phase is 550 cSt Sylgard 184 PDMS (1:1 volume ratio of base to curing agent).

Within the trials performed with 1% SDS the Đ ranged from 1.00% to 8.25%, whereas with 5% Kolliphor the Đ ranged from 1.09% to 11.50%. Within the 1% SDS trials 72% of the Đ s were less than 3% and therefore considered highly uniform (Wu et al., 2014), whereas within the Kolliphor trials only 55% of the Đ s were less than 3%.

2.3.2 FIET size

Using 1% SDS as the continuous phase produced FIETs ranging from 110 to 400 μm in diameter, while the 5% Kolliphor continuous phase produced diameters of 67 to 117 μm.

Table 2.2: Average diameters of fluorescent implantable elastomer tags produced by microfluidic chips with a continuous phase of 1% sodium dodecyl sulfate (N=3) compared to those with a continuous phase of 5% Kolliphor (N=3).

Flow Rates (μL min^{-1})		Average Diameter (μm) ± SEM	
Disperse	Continuous	1% SDS	5% Kolliphor
1	100	401 ± 35	117 ± 10
1	200	327 ± 32	95 ± 6
1	300	281 ± 30	82 ± 4
1	500	229 ± 21	67 ± 2
0.5	100	329 ± 50	114 ± 12
0.5	200	213 ± 75	91 ± 7
0.5	300	165 ± 68	80 ± 4
0.5	500	134 ± 51	67 ± 3
0.25	100	221 ± 77	120 ± 9
0.25	200	173 ± 61	98 ± 6
0.25	300	146 ± 45	85 ± 3
0.25	500	110 ± 27	70 ± 2

The average diameters of FIETs produced by each microfluidic chip at the tested flow rates can be found within appendix B of this thesis (fig. B1-B6).

2.3.3 Ratiometric response to PO_2

The FIETs' were exposed to humidified N_2 and O_2 gas mixtures ranging from 0 to 0.2 atm PO_2 to assess their response and construct a calibration curve. The fluorescence intensity of the indicator and reference dyes was measured and background fluorescence accounted for (fig 2.8). The fluorescence of the indicator dye was quenched by O_2, whereas the fluorescence of the reference dye remained unchanged (fig. 2.9).

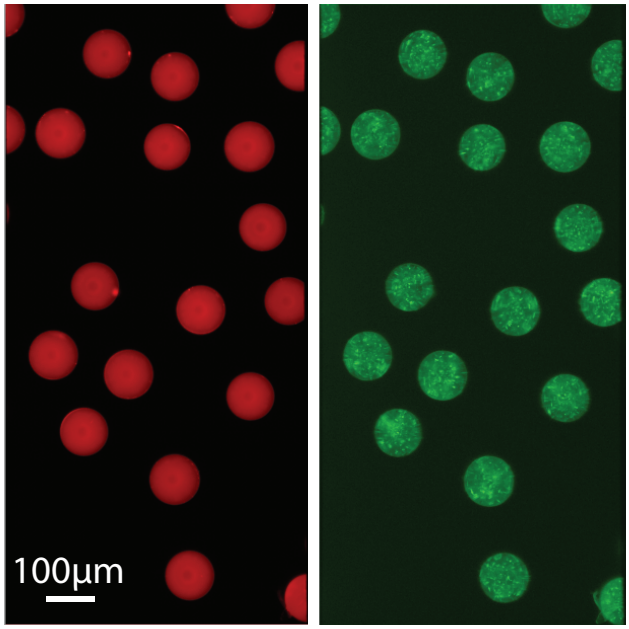

Figure 2.8: An example of the images of the FIETs taken using a Gemini Image Splitter (10×). On the left is the fluorescence of the indicator dye passed through the long wavelength filter (>620 nm), on the right is the fluorescence of the reference dye passed through the short wavelength filter (< 570 nm). Images have been edited from grey scale to colour.

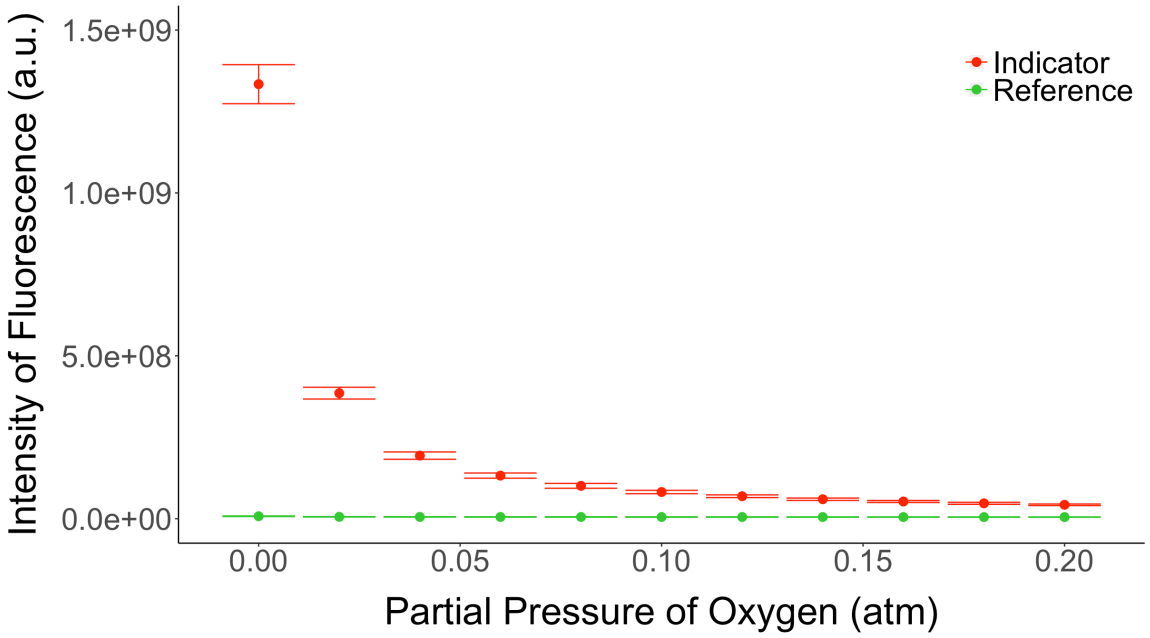

Figure 2.9: The mean corrected total fluorescence (± S.E.M) of the indicator dye (PtTFPP) and the reference dye (F8BT) in response to changing PO_2 concentrations (N=24).

From the corrected total fluorescence of the indicator dye, a Stern-Volmer plot was made by normalizing the fluorescence intensities of the indicator dye to its maximum fluorescence in 0 atm O_2. The ratio of the indicator dye's fluorescence in the absence of O_2 to its fluorescence in PO_2 is referred to as R0.

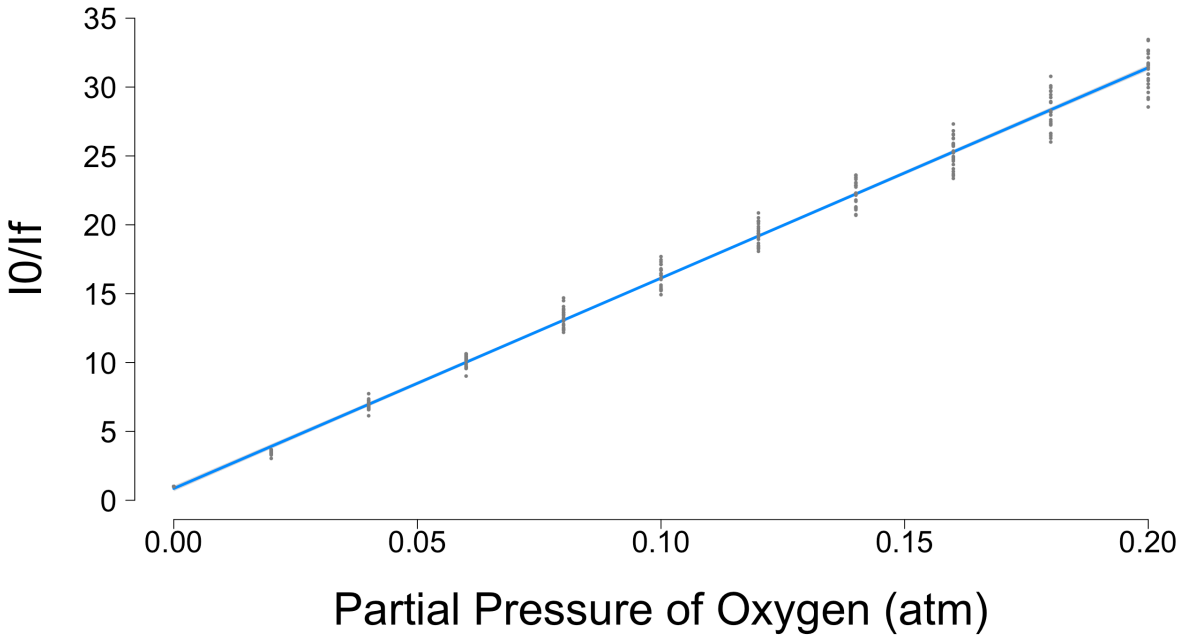

Figure 2.10: A Stern-Volmer plot of the indicator dye fluorescence without the reference dye in response to increasing partial pressure of O_2 (atm) within humidified gas mixtures of N_2 and O_2. I0 is the fluorescence of the dye in the absence of the quencher, and If is the fluorescence at each respective PO_2 tension; the ratio of these two values is R0.

The equation of the linear model fit through the Stern-Volmer plot of the indicator fluorescence is $y = 1.53x + 0.86$, with a regression coefficient (R^2) value of 0.9923. The next step was to construct a calibration curve of the FIETs using the reference dye. The fluorescence of the reference dye at a given PO_2 was divided by the corresponding fluorescence of the indicator dye. This ratio is referred to as R1.

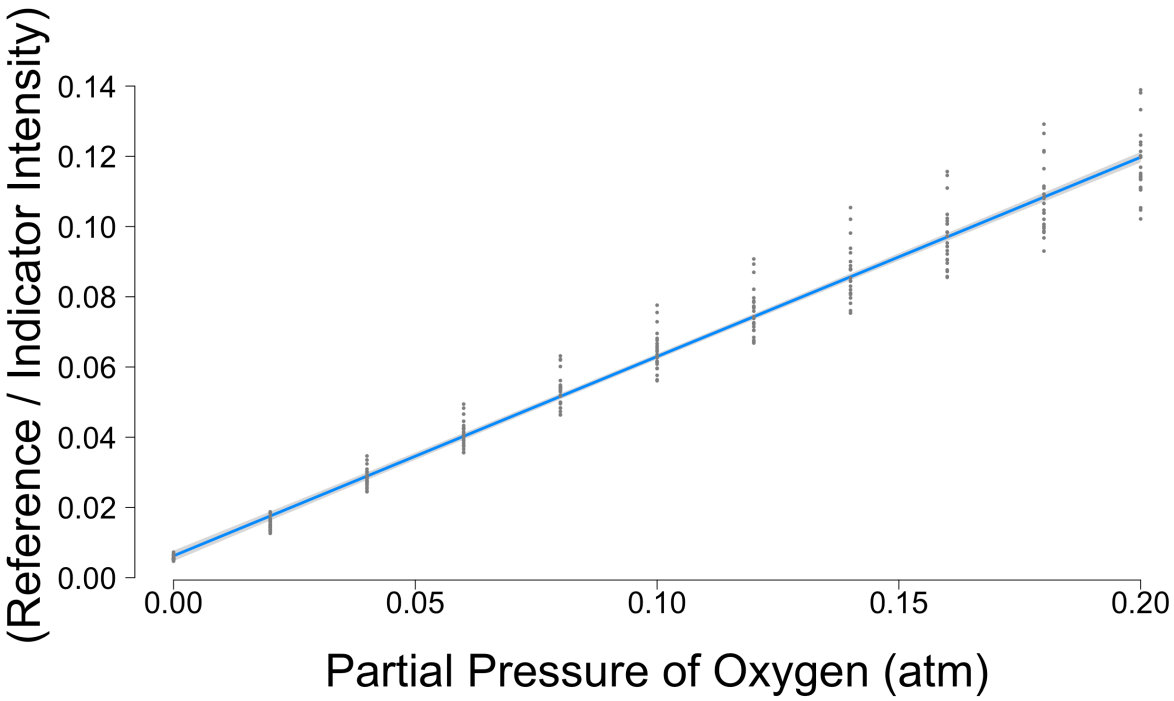

Figure 2.11: The change in the ratio of reference to indicator fluorescence (R1) of FIETs (*N*= 23) to increasing partial pressure of oxygen (atm) within humidified gas mixtures of N_2 and oxygen.

R1 exhibited a linear response to increasing PO_2 concentration. The equation of the linear model fit to the data is $y = 5.7\times10^{-3}x + 6.3\times10^{-3}$, with a R^2 value of 0.963. The next step is to normalize R1 to its fluorescence in the absence of a quencher ($R1_0$). The ratio of $R1_0$ to R1 is referred to as R2.

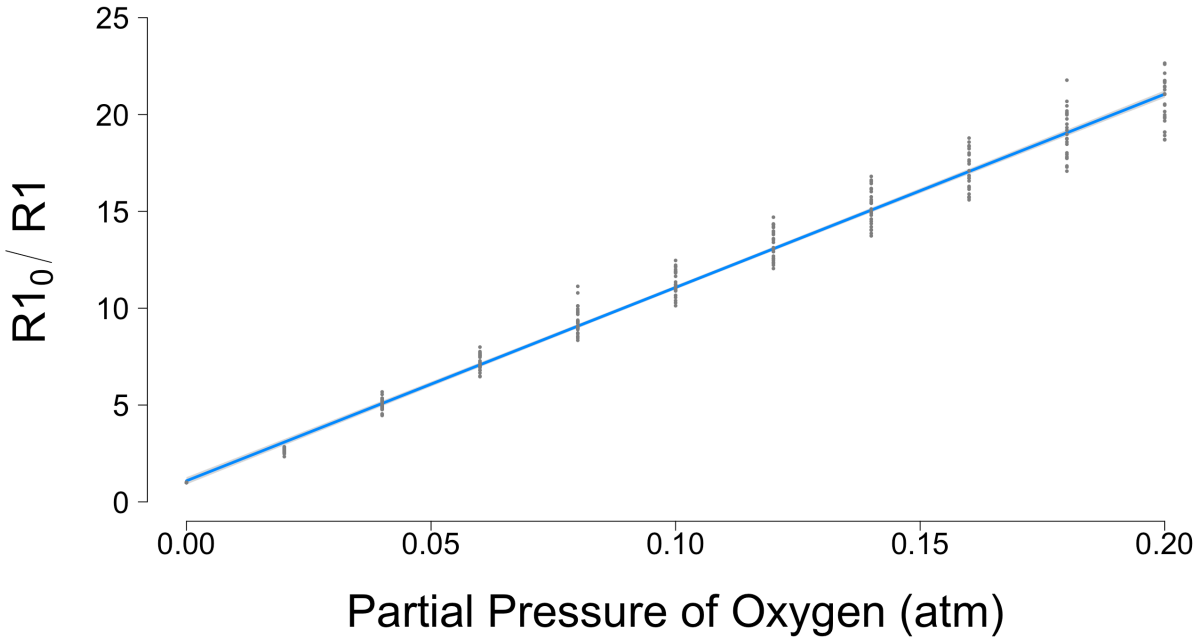

Figure 2.12: Stern-Volmer plot of the FIETs' response to increasing partial pressures of oxygen in hydrated gas mixtures of O_2 and N_2 (N=24). R1 is the ratio of the reference dye to indicator dye in the respective PO_2 and $R1_0$ is the ratio of the reference dye to indicator dye in the absence of O_2; the ratio of $R1_0$ to R1 is referred to as R2.

Within the Stern-Volmer plot of R2 the R^2 value is 0.9839 and the equation of the linear model is y = 99.83x+1.09. Having fit all three linear models, I made a comparison of their R^2 values and equations (table 2.3). I also examined the difference in the coefficient of variation of measurements at 0.04, 0.1, 0.16 and 0.2 atm PO_2 for R0, R1 and R3 (table 2.4).

Table 2.3: A comparison of the linear models fit for the Stern-Volmer plot of the fluorescence of the indicator dye (R0), the ratio of the reference dye to the indicator dye (R1) and the Stern-Volmer plot of the ratio of the reference dye to the indicator dye (R2).

Plot type	R^2	m	b
R0	0.9923	1.53	0.86
R1	0.963	5.7×10^{-3}	6.3×10^{-3}
R2	0.9839	99.83	1.09

Table 2.4: A comparison of the coefficient of variation within measurements of the Stern-Volmer plot of the fluorescence of the indicator dye (R0), the ratio of the reference dye to the indicator dye (R1) and the Stern-Volmer plot of the ratio of the reference dye to the indicator dye (R2).

	Coefficient of Variation (%)			
Plot Type	0.04 atm	0.1 atm	0.16 atm	0.2 atm
R0	4.70	4.85	4.43	4.34
R1	9.23	8.76	8.82	8.32
R2	6.17	5.94	5.92	5.96

2.3.4 Photodegradation of the indicator and reference dye

The FIETs were continuously illuminated with 390 nm light for 60 seconds to test their resilience to photodegradation.

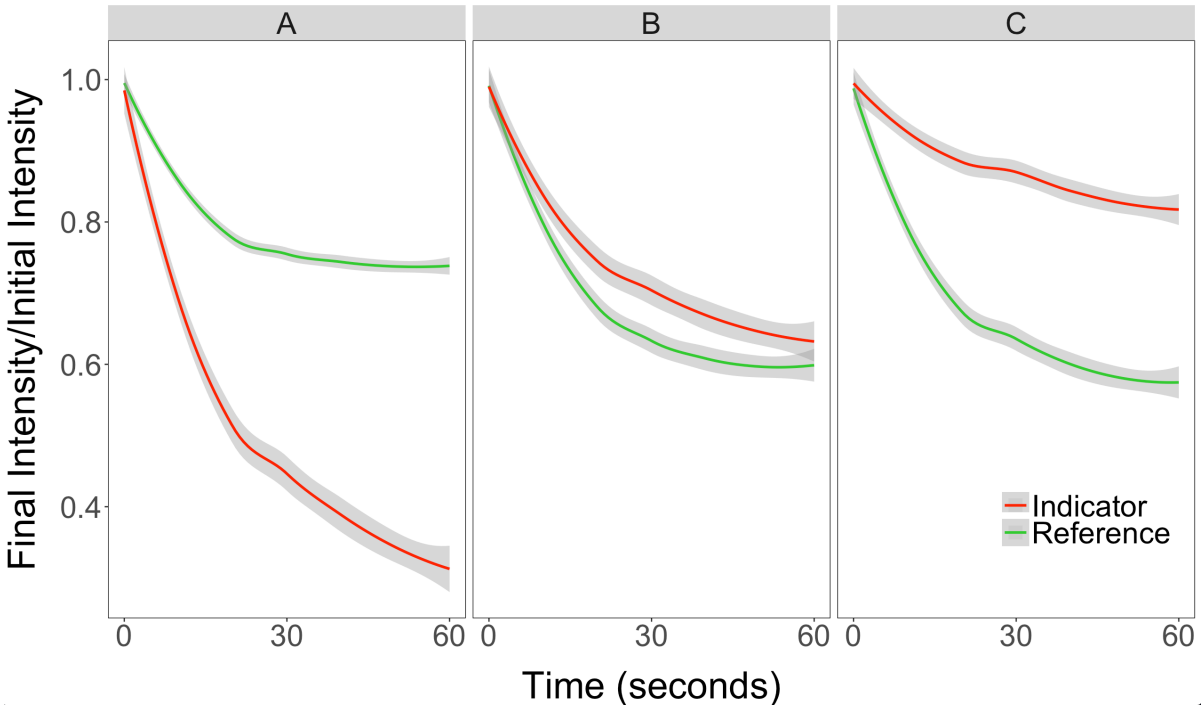

Figure 2.13: The change in the indicator (PtTFPP) and reference (F8BT) fluorescence of FIETs (*N*=5) relative to initial fluorescence within 0.02 (A), 0.1 (B) and 0.2 (C) atm oxygen in a humidified gas mixture of oxygen and N_2 following 60 seconds of constant illumination with 390 nm light.

When held within a steady-state environment of 0.02 atm O_2, the indicator dye's fluorescence degraded to 31.3 ± 1.5% of its initial value, whereas the reference dye degraded to 74.0 ± 0.8% of its initial value. In the 0.1 atm O_2 environment the indicator dye degraded to 62.9% ± 1.8% of its initial value and the reference dye degraded to 59.5 ± 1.3% of its initial value. In the 0.2 atm O_2 environment the indicator dye's fluorescence degraded to 82.2 ± 1.0% of its initial value and the reference dye degraded to 57.6 ± 0.9% of its initial value.

A figure of the indicator and reference dyes' fluorescence after 10 minutes of continuous excitation can be found in appendix C of this thesis (fig. C1).

2.3.3 Drift within PO_2 measurements

The fluorescence intensities of the FIETs in each of these O_2 tensions (0.02, 0.1 and 0.2 atm) were converted into PO_2 values using the equation of the line from the model fit to R1.

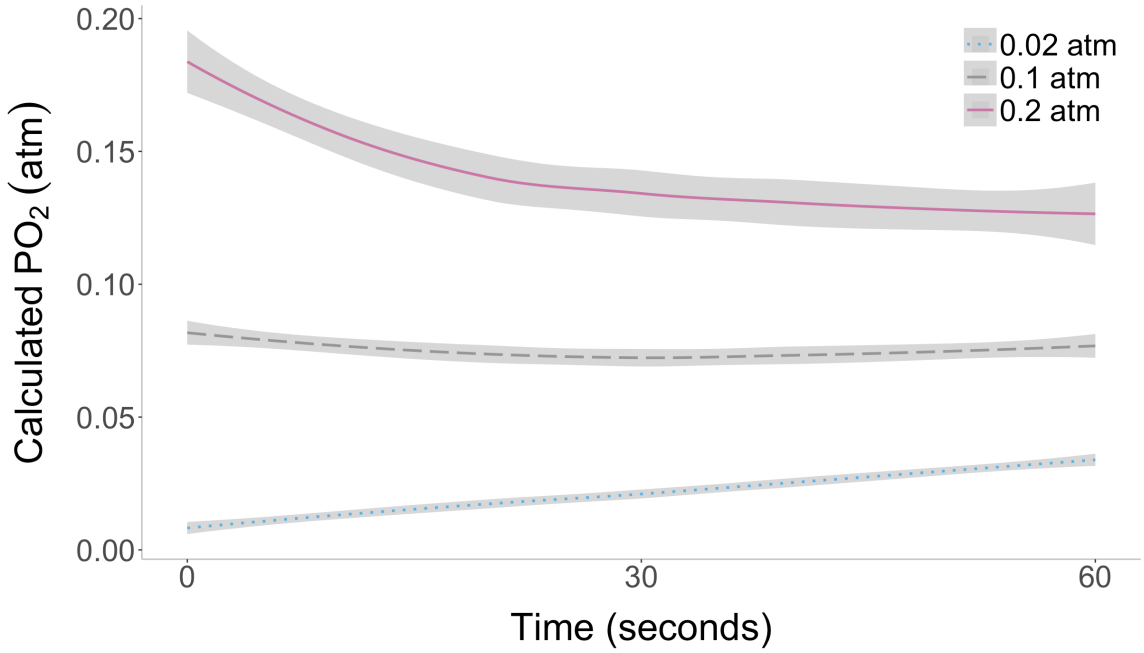

Figure 2.14: Drift within the calculated percent oxygen measurements (based off of the equation of the linear model in R1; $y = 5.7\times10^{-3}x + 6.3\times10^{-3}$) of FIETs held within 0.02, 0.1 and 0.2 atm oxygen in a humidified gas mixture of oxygen and N_2, following 60 seconds of constant illumination with 390 nm light.

Within a 0.2 atm O_2 environment, the FIETs' measurements drifted downwards by 31.6 ± 0.82%. Within the 0.1 atm O_2 environment, the FIETs' measurements drifted

downwards by 6.1 ± 1.4%. Finally, in the 0.02 atm O_2 environment the FIETs' measurements drifted upwards by 359.7 ± 66.2%.

2.3.4. Measuring PO_2 *in situ*

In order to measure a PO_2 within an agar gel, a calibration curve was made by sequentially exposing the FIETs to gas mixtures of 0.2, 0.1 and 0 atm PO_2 in N_2.

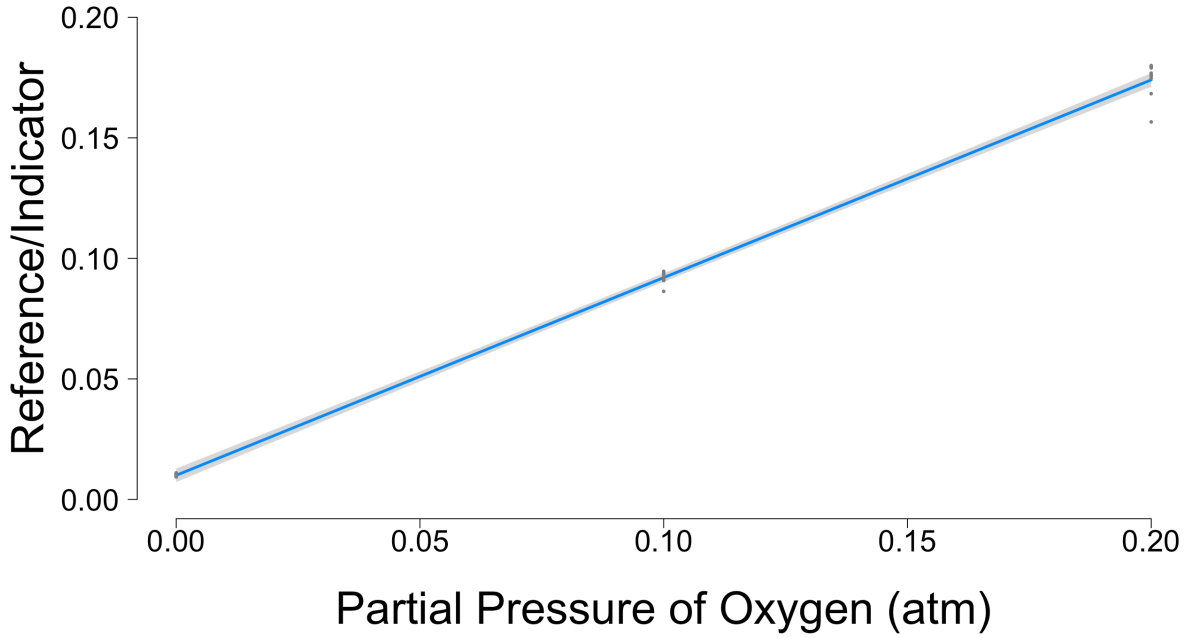

Figure 2.15: The calibration curve for the FIETs used in measuring the partial pressure of oxygen within a 0.5% agar gel bridge (N=8). FIETs were sequentially exposed to 0.2, 0.1 and 0 atm PO_2 gas mixtures of nitrogen and oxygen.

The equation of the linear model fit to the calibration curve is y=0.820096x + 0.010020 and R^2=0.9959. The equation of the line was used to calculate PO_2 from the FIETs embedded in a block of agar. The first measurements were taken before an O_2 gradient was established (Time 0) and the second measurements were taken after N_2 gas and air had been flowing on either side of the agar for 20 hours (Time 1) (fig. 2.16).

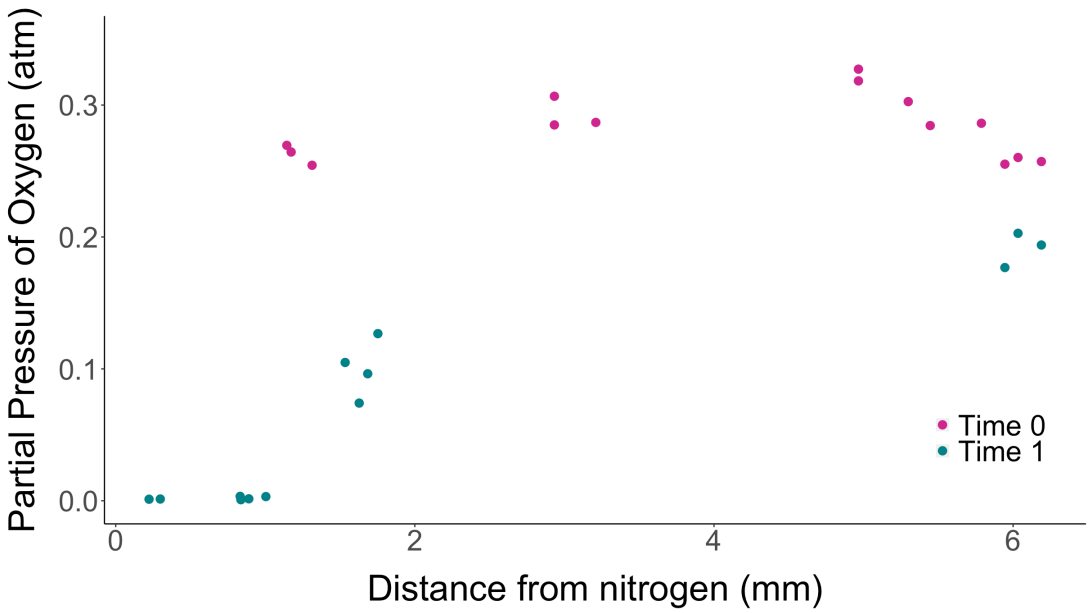

Figure 2.16: The measurement of partial pressure of oxygen (in atmospheres) within a 0.5% agar gel by the FIETs. Time 0 (N= 14) indicates the measurements taken before nitrogen and air flowed on either side of the agar. Time 1 refers to measurements taken after the gases had been flowing for 20 hours (N=14).

The FIETs' distance was measured relative to the edge of the agar block exposed to the N_2 compartment. The FIETs were separated into three areas: those greater than 5 mm from the N_2 edge (and therefore close to the edge exposed to air), those between 1.3 mm and 5 mm (in the middle of the agar), and those less than 1.3 mm away from the N_2 edge. The average PO_2 calculation ± SEM from the FIETs was calculated for each area (table 2.5).

Table 2.5: Average calculated PO_2 (atmospheres ± SEM) from FIETs within 0.5% (w/v) agar gel at different distances. Time 0 indicates measurements taken before an oxygen gradient was established within the gel. Time 1 indicates measurements taken 20 hours into oxygen gradient formation.

	Distance (mm)		
Time	x>5	1.3<x<5	x<1.3
0	$0.27 \pm 8.0\times10^{-3}$	$0.30 \pm 8.4\times10^{-3}$	$0.26 \pm 4.4 \times10^{-3}$
1	$0.19 \pm 7.6\times10^{-3}$	$0.10 \pm 1.3\times10^{-2}$	$2.0\times10^{-3} \pm 4.0\times10^{-4}$

2.4 Discussion

The objective of this thesis was to develop a novel method for the measurement of PO_2 within insects. Fibre-optic probes are currently the preferred method for measuring PO_2, but have several limitations – insects need to be tethered, immobilization causes stress and a probe can only measure PO_2 at one location at a time. The FIETs proposed within this study would theoretically allow for animals to move freely during PO_2 measurements, reduce stress from immobilization, and be able to take measurements from multiple locations simultaneously (providing spatially specific PO_2 information).

There were four objectives laid out for these FIETs at the beginning of this thesis. First, they must be uniformly sized with a diameter of 70 μm or less. Secondly, the ratiometric dye system must exhibit a linear response to PO_2. Thirdly, the FIETs must be photostable enough to obtain meaningful PO_2 measurements. Fourthly, and finally, the FIETs must be able to operate within an autofluorescent system.

The data show that uniform emulsions with FIET diameters as small as 67 μm were achieved with the microfluidic chip, but changes to the chip design could potentially allow for even smaller FIETs. The ratiometric dye system did exhibit a linear response to PO_2, with

a maximum R^2 value of 0.984. The FIETs also exhibited photodegradation over 60 seconds of constant illumination, but to a degree that is manageable within the experimental set up. Finally, the FIETs were able to measure PO_2 within an autofluorescent system and detect a PO_2 gradient, showing promise for *in vivo* trials.

2.4.1 Uniformity of emulsions

The data show that the microfluidic chip produces highly uniform emulsions when using either Kolliphor or SDS as a surfactant. In this study, I assumed that the surfactant itself would not have an effect on flow regime or microsphere size. Therefore, a comparison in non-uniformity and microsphere size range was made between microfluidic chips using 1% SDS and 5% Kolliphor. Overall, the microfluidic chips using 1% SDS produced more uniform batches (72%) compared to the chips using Kolliphor (55%). This is likely due to the fact that using a less viscous continuous phase often results in a dripping regime rather than a jetting regime (Utada et al., 2005). In dripping, the droplets of disperse phase are formed at the injection tube tip and are immediately swept away by the continuous phase. This point of droplet formation is commonly referred to as the 'pinch-off point'. When the viscosity of the continuous phase is increased, so too are the viscous forces operating around the tip of the injection tube. This results in the continuous phase 'dragging' the pinch-off point further down the collection tube (fig. 2.15).

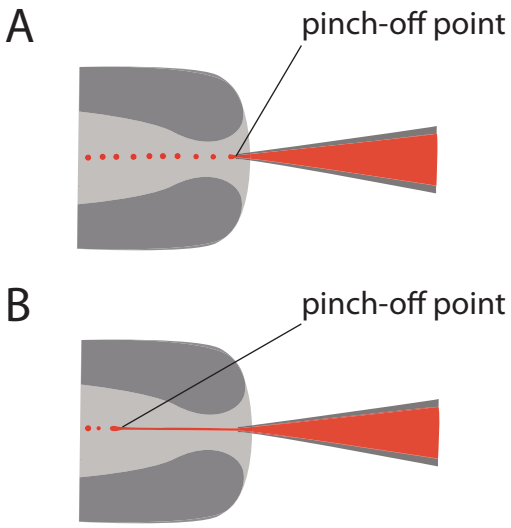

Figure 2.15: Droplet formation in dripping (A) and jetting (B) regime within a microfluidic chip. Within a jetting regime the pinch-off point is pulled further down the collection tube, whereas in the dripping regime the pinch-off point is at the tip of the injection tube.

When the pinch-off point is dragged further down the collection tube an unstable cylinder of disperse phase is formed behind it, which is subject to Rayleigh-Plateau instability. This refers to the phenomenon of a non-viscous fluid stream becoming more unstable over time as it lengthens, eventually breaking into droplets (Rayleigh, 1878). This is due to small perturbations within the fluid stream, which build until as the jet grows longer it reaches maximum instability and separates into smaller droplets (Rayleigh, 1878; Tomotika, 1935). Investigations into this phenomenon were originally focused on low-viscosity fluids (such as water dripping from a tap), but have also been explored within the context of a viscous jet surrounded by another viscous fluid (Tomotika, 1935), just like within a microfluidic chip. Because of the formation of this unstable jet, a jetting regime will produce less uniform emulsions than a dripping regime (Shah et al., 2008; Utada et al., 2005). This would also explain why the Kolliphor trials had a wider range of Đs (1.09-11.50%) compared to the SDS trials (1.0-8.25%).

Overall, the SDS trials produced larger microspheres than the Kolliphor trials, so Kolliphor was deemed a more appropriate surfactant for the FIETs. Furthermore, variation was lower between the microfluidic chips in the Kolliphor trials than the SDS trials, indicating more predictable flow regimes. Kolliphor also dissolves more readily into water than SDS, so it was possible to increase its concentration (up to 10% w/v) in the continuous phase when making the FIETs. With a more viscous continuous phase I was able to produce even smaller microspheres without impacting their curing. It should be noted that curing of the FIETs was impacted when their diameter dropped below 70 μm, but a literature search failed to yield any explanation as to why the size may impact curing. Interestingly, when the FIET material was vortexed (producing a non-uniform emulsion) FIETs smaller than 70 μm were able to cure. This suggests that a property of the microfluidic chip is preventing the FIETs from curing. For more information on the operation of the microfluidic chip, refer to appendix D at the end of this thesis.

2.4.2 The ratiometric dye system and response to PO_2

From figure 2.8, it is evident that the fluorescence of PtTFPP is quenched with increasing PO_2: very bright fluorescence is observed in anoxia that dramatically falls with the introduction of 0.02 atm O_2 and then plateaus as PO_2 increases linearly. Previous studies that have used PtTFPP have used a Stern-Volmer plot to transform the quadratic relationship of fluorescence and PO_2 to a linear one (Jiang et al., 2012). When using a Stern-Volmer plot, the fluorescence intensity of the indicator dye (PtTFPP) in different PO_2s is normalized to the maximum fluorescence intensity produced in the absence of O_2. A linear relationship can also be achieved, and in some cases improved, when a reference dye is incorporated into the

sensor (Cao et al., 2004). To see if the FIETs' reference dye improved linearity, I made two Stern-Volmer plots: one with the reference dye fluorescence (R2) and one with just the indicator dye fluorescence (R0). To compare the goodness of fit between the two plots I used the R^2 value, which is also a reflection of linearity. The R^2 value measures the proportion of variation in the response variable (the fluorescence ratio of the dyes) accounted for by the explanatory variable (Whitlock and Schluter, 2015). The closer the R^2 is to 1 the better the fit of the model and the more linear the relationship. The R^2 value of the R0 plot is 0.9923, while the R^2 value of the R2 plot is 0.9839. The total percent change in linearity following the incorporation of the reference dye is a 0.84% decrease. The decrease in linearity is likely due to heterogeneity introduced into the FIET matrix by the reference dye (Bedlek-Anslow et al., 2000; Hughes and Douglas, 2006). Although the aggregation of the reference dye within the matrix may appear minimal, at the microscale it is large enough to introduce differences between the FIETs and thus affect the linearity of the model. Although this is not ideal, a change of only 8.4% shows that linearity is minimally impacted with the introduction of the reference dye. This decrease in linearity is a trade-off for the reference dye's ability to account for scattering and interference during measurement. Overall, the reference dye will allow for more accurate measurements of O_2 within an animal, but may impact the precision of those measurements.

Using a Stern-Volmer plot for calibrating the FIETs requires measuring their fluorescence in the absence of O_2 to produce a reference R0 for each bead. However, this is not always feasible for applications *in vivo,* as exposing an animal to 0 atm O_2 would cause physiological damage or death and undoubtedly affect future PO_2 measurements. It would be possible to obtain a 0 atm measurement if the animal was sacrificed after taking desired PO_2

readings, but this could limit the range of applications for the FIETs. Using a reference dye means that a linear relationship between PO_2 and the FIETs' fluorescence is still achieved without having to take a measurement in anoxia (0 atm O_2). The R^2 value of the linear model fit to the R1 ratio change in response to PO_2 is 0.963, which is a 2.2% decrease in linearity compared to the model fit to R0. A self-referential system, like the one used in R0, will always result in higher linearity, but a 2.2% decrease can easily be tolerated. One drawback of using the R1 ratio is the spread of the measurements at each PO_2 tension. From table 2.4, the R1 ratio has the highest coefficient of variation at each PO_2 tension compared to R0 and R2. This spread of measurements reduces the precision of the FIETs, making it difficult to discern subtle changes in PO_2, particularly at higher PO_2 tensions. For instance, the highest R1 value of the FIETs within 0.16 atm PO_2 is 0.12, while the lowest R1 value of the FIETs in 0.2 atm PO_2 is 0.10. This overlap between the measurements makes it difficult to distinguish if a FIET is reading 0.18 atm O_2 or 0.2 atm O_2. However, at lower PO_2 tensions there is no overlap of measurements, the highest R1 value at 0.04 atm O_2 is 0.034 and the lowest R1 value at 0.1 atm O_2 is 0.56. While the coefficients of variation are smaller for R2 and R0, overlapping of measurements between different PO_2 tensions was still observed. Therefore, the FIETs are suitable for detecting large changes in PO_2, but not appropriate for measuring subtle ones above 0.1 atm O_2.

2.4.3 Photodegradation

It is an unfortunate fact that all dyes are altered by light over time, and the dyes used within this project are no exception. Both the indicator dye and reference dye faded in response to continuous illumination of the excitation light, and the degree of

photodegradation was dependent upon the PO_2 tension. Within the 0.02 atm PO_2 tension the indicator dye degraded almost threefold more than the reference dye, while the opposite trend was observed within the 0.2 atm PO_2 environment. The degree of photodegradation was approximately equal between the dyes within the 0.1 PO_2 tension. Ideally the degree of photodegradation of the two dyes would be the same across all three PO_2 tensions, as this would keep the ratio of reference dye to indicator dye consistent and reduce drift within the PO_2 measurements.

The unequal degree of photodegradation between the indicator dye and the reference dye leads to an apparent drift in the PO_2 value calculated from the fluorescence of the FIETs. Because the ratio of reference dye to indicator dye remains fairly consistent in the 0.1 atm PO_2 tension the overall drift is minimal (only 6.1%). However, the drift in measurements is exacerbated within the 0.02 atm and 0.2 atm PO_2 environments, which is due to the difference in photodegradation of the reference and the indicator dyes. Over the course of 60 seconds, the measurements within the 0.2 atm PO_2 tension drifted by 31.6% while the measurements within the 0.02 atm PO_2 drifted by 359.7%. Initially, these results seem to pose a problem. How can these FIETs provide accurate measurements of PO_2 if their measurements drift so much? However, it is important to place these measured rates of photobleaching in the context of the duration of excitation light exposure required to take a measurement. At the same level of excitation light intensity used in the photobleaching experiments, the FIETs can be imaged by the camera in 25.05 ms. Thus, using this exposure duration, I could theoretically capture 1197 measurements within 30 seconds of illumination. By carefully meting out the excitation illumination during measurements and protecting the FIETs from ambient light, the effect of photodegradation can be minimized.

2.4.4. Measuring PO_2 *in situ*

Obtaining meaningful measurements of PO_2 *in situ* is the first step to preparing the FIETs for use *in vivo*. I initially tried extracting fluorescence data from the FIETs within the agar in the same way that I had when I constructed the first calibration curves (fig. 2.10 – fig. 2.12), by subtracting the background fluorescence from the FIETs' fluorescence. However, this was not deemed an appropriate approach for measuring PO_2 within our agar set-up. The agar gel did exhibit bright autofluorescence during imaging, but FIETs imaged within the agar were resting on the glass slide. Therefore, the agar autofluorescence did not interfere with the background fluorescence. Because the background fluorescence was different in the agar compared to the glass slide during the calibration, subtracting background fluorescence resulted in inaccurate measurements. Therefore, uncorrected integrated density was used to construct the calibration curve and extract information from the FIETs within the agar. Validating the PO_2 of the agar gel during or immediately after the measurements would help confirm whether this was an appropriate approach or not.

I made two predictions of the FIETs performance within the agar gel. Firstly, that at Time 0 (before an O_2 gradient was established) the FIETs would read approximately 0.21 atm PO_2 regardless of their location within the gel. Secondly, that at Time 1 (after N_2 gas and air had been flowing on opposite sides of the gel for 20 hours) the FIETs closer to the N_2 edge of the gel would read a lower PO_2 value compared to those on the edge exposed to air, indicating that an O_2 gradient was established. If these predictions were correct, it would provide evidence that a change in fluorescence of the FIETs within the agar was due to the presence of a PO_2 gradient and support the feasibility of using them *in vivo* to measure PO_2. An alternative hypothesis is that any change in fluorescence between Time 0 and Time 1 is

due to photobleaching. If this hypothesis were correct then I would expect to see an overall decrease in fluorescence between Time 1 and Time 0, but no difference in PO_2 readings across the width of the gel at Time 1.

In terms of my first prediction, the FIETs all read approximately the same: The FIETs read 0.26 atm PO_2 on the N_2 side of the gel, 0.30 atm PO_2 in the middle of the gel and 0.27 atm PO_2 on the edge exposed to air. While these values are all approximately the same, they are much higher than expected. The most likely explanation for this is that the gel was still warm when the Time 0 measurements were taken, and that temperature had an effect on the FIETs' readings. PtTFPP is quenched by O_2 via collisional quenching, an increase in temperature will cause a faster diffusion rate and more collisions, resulting in more quenching (Lakowicz, 2006). It would be useful to repeat the experiment and validate the PO_2 and the temperature of the agar during measurements with the FIETs. It would also be worthwhile to quantify the effect of temperature on the FIETs' fluorescence. While the FIETs' higher PO_2 reading was unexpected, my prediction that the PO_2 reading would not change across the width of the gel at Time 0 was met.

In terms of my second prediction, at Time 1 the FIETs near the N_2 edge read 1.9×10^{-3} atm PO_2, in the middle they read 0.10 atm PO_2 and near the edge exposed to air they read 0.19 atm PO_2. From these readings, it is clear that at Time 1 the FIETs' measurements of PO_2 decrease as they approach the edge of the gel exposed to N_2, thus my second prediction was met. These two predictions support the hypothesis that the change in fluorescence of the FIETs between Time 0 and Time 1 is due to a change in PO_2 levels within the gel, rather than photodegradation or some other confounding factor. Validating the PO_2 levels within the gel at Time 1 with a fibre-optic probe would strengthen the evidence for this hypothesis. In

addition, repeating a control gel in which air and N_2 did not enter the chamber between Time 0 and Time 1 could potentially rule out the alternative hypothesis that a change in fluorescence is due to photodegradation. However, the photodegradation hypothesis is already fairly weak given that there is a difference in PO_2 along the width of the gel at Time 1.

3: Conclusions and future directions

While the results within this thesis are promising, there is room for improvement within the microfluidic chip and FIET design. Furthermore, there are important considerations that need to be made before implanting the FIETs within an animal. I will now compare the microfluidic chip and FIETs within this thesis to those in similar studies, suggest improvements and propose steps that need to be taken to move towards *in vivo* trials.

3.1: Comparisons to other studies

3.1.1 Microfluidic devices and approaches

The methods used to produce emulsions and implantable O_2 sensors can range from complex and expensive to simple and cheap, depending on the specifications of the emulsions. For instance, multi-layered droplets are often used for drug delivery, and require complex microfluidic chips to produce (Shah et al., 2008). For solid microspheres (such as the FIETs made in this study), much simpler methods may be used. The microfluidic chip built within this thesis was based on previous pulled microcapillary devices (Er Qiang et al., 2014; Utada et al., 2005). Previous microfluidic devices have fared better in terms of uniform emulsions compared to the one built in this thesis. Both Utada et al. (2005) and Er Qiang et al. (2014) built microfluidic devices with Đs under 3%, with no mention of any emulsions exceeding that value. While up to 72% of emulsions within my microfluidic chip had a Đ of less than 3% (when using 1% SDS as the continuous phase), there were also emulsions produced with Đs of up to 8.25%. When using 5% Kolliphor® as the continuous phase only 55% of emulsions produced had a Đ of under 3%. The lack of uniformity compared to other studies given the amount of work to make each microfluidic chip is disappointing –

investigating alternative and simpler methods of producing uniform FIETs would be a worthwhile venture.

Previous work has simplified coaxial flow chips to a hypodermic needle inserted into a segment of PTFE tubing (Nurumbetov et al., 2012; Quevedo et al., 2005). The disperse phase flows through the hypodermic tubing, while the continuous phase flow through the segment of PTFE. This configuration reduces issues with clogging and results in an overall higher yield of droplets (Nurumbetov et al., 2012). Because of its simple design, it requires little set up and can easily be disassembled and rebuilt if clogging does occur while droplets are being made. The microfluidic device made by Nurumbetov et al. (2012) was able to produce core/shell droplets ranging from 282 μm to 418 μm, whereas my microfluidic device produced solid microspheres ranging from 70 μm to 117 μm when using 5% Kolliphor® as the continuous phase. However, adapting Nurumbetov et al.'s design for solid microspheres and manipulating flow rates may further reduce the size of droplets (2012).

Other studies have completely bypassed a microfluidic chip by either using an emulsification membrane or an emulsion polymerization approach. An emulsification membrane works by passing the disperse phase through a porous membrane with the continuous phase flowing over the surface (Piacentini et al., 2014). This method produces a high yield of non-uniform droplets with Đs often greater than 10% (Vladisavljević et al., 2012). An emulsion polymerization approach refers to adding polymer monomers, surfactant and continuous phase to a reaction chamber. With added heat the monomers will polymerize and form solid microspheres (Cao et al., 2004). Emulsion polymerization results in a highly uniform emulsion (Đs under 3%) and boasts a high yield of droplets, but this method limits the range of matrices that may be used and requires specialized equipment.

For the purpose of this project, the microfluidic chip is functional but does not deliver the uniformity of droplets shown in other studies. An alternative for the future should be easy to assemble and still deliver highly uniform emulsions.

3.1.2. FIETs and other O_2 sensors

The FIETs within this study can be compared to other micro-sized O_2 sensors in three respects: their photostability, their response to PO_2, and their demonstrated use *in situ*. In terms of photostability, the FIETs made within this study are less stable when compared with other micro-sized O_2 sensors. For instance, Collier et al. shows a drift in O_2 measurements of less than 1% after 10 hours of constant illumination (2011). This study is similar to my thesis in that a porphyrin compound is used as an O_2 indicator and incorporates a reference dye into the sensor (Collier et al., 2011). Similarly, another study using a platinum porphyrin compound as the indicator dye reported a 5% drift in O_2 measurements following 30 minutes of constant excitation (Cao et al., 2004). Within Collier et al.'s study the intensity of the excitation light source was 15.27 $\mu W\ cm^{-2}$ (2011), but I was unable to measure the intensity of the excitation light used within my own research. It is possible that the intensity of the excitation light used within this thesis is far greater than what has been used in other studies. Reducing the intensity of the excitation light could potentially improve the photostability of the FIETs and make them comparable to other micro-sized O_2 sensors.

The FIETs within this study exhibited a linear response to increasing PO_2 tensions. This linear response to O_2 has been shown in previous studies using PtTFPP as an indicator dye (Jiang et al., 2012). My FIETs are most comparable to those produced by Cao et al. in that they contain a ratiometric dye system and a metalloporphyrin compound as the indicator

dye (2004). Within Cao et al.'s study, they use a Stern-Volmer plot to calibrate their sensors, eschewing the ratio of reference dye:indicator dye (2004). The R^2 value of the Stern-Volmer plot within their study is 0.997 (Cao et al., 2004), exhibiting a similar degree of linearity compared to the Stern-Volmer plot within this study (R^2=0.984). The slightly higher R^2 value within the Cao et al study is possibly due to their reference dye being more soluble in their PDMA matrix than my reference dye was in the PDMS matrix of the FIETs (Cao et al., 2004). Although no empirical values of solubility are given, the study mentions that the solubility of the indicator dye and reference dye are roughly equal, which was not observed within my thesis (Cao et al., 2004). Having a more homogenous distribution of the reference dye could reduce micro-heterogeneity within the FIETs, thus increasing the consistency of the PO_2 response and improving linearity. However, it must be noted that the difference between the R^2 values is very small. Overall, the FIETs within this study exhibit a highly linear response to PO_2.

Cao et al. also demonstrated the use of their sensors within an autofluorescent system, using human plasma which autofluoresces within the same wavelength as their reference dye (600-650 nm) (2004). Similarly, within this study the agar autofluoresced within the same wavelength as the reference dye (550 nm). However, within Cao et al.'s study, the sensors were not used to gain spatially specific information as their fluorescence was measured within a spectrophotometer rather than imaged with an inverted fluorescence microscope (2004). Other studies have tried to measure O_2 using imaging rather than spectroscopy, although none have attempted to measure an O_2 gradient within a biologically relevant system (Collier et al., 2011; Wu et al., 2009). In this respect, my thesis is unique in that it demonstrates the FIETs viability *in situ* using agar and potentially *in vivo*, whereas other

studies have only constructed calibration curves and speculated on their use *in vivo* (Collier et al., 2011; Jiang et al., 2012; Li et al., 2015). Demonstrating the FIETs' use within an autofluorescent system is an important step forward, but there are other factors that need to be considered before the FIETs are implanted within an animal.

3.2 Moving towards biological measurements

My thesis serves as the foundation of a larger research goal, which is to implant the FIETs within a living organism and obtain meaningful PO_2 measurements. A critical component of moving towards implanting the FIETs within an animal is establishing their biocompatibility. Ideally, implantation of the FIETs should not elicit a local or systemic response from the animal.

There are several ways to test the biocompatibility of FIETs within model insects, the most notable being immune response and mortality. The insect immune response can be divided into two categories: humoral defenses and cellular defenses (Lavine and Strand, 2002). The humoral defenses consist of the secretion of antimicrobial peptides, whereas cellular defenses consist of encapsulation and melanogenesis of foreign bodies (Lavine and Strand, 2002; Tsuzuki et al., 2014). Because FIETs are an implanted foreign body, evaluating the cellular immune response of insects to the FIET material will be particularly important. Once a foreign body is recognized by the insect's immune system, phenyloxidase (PO) enzyme production is activated to begin encapsulation (Lavine and Strand, 2002; Ratcliffe et al., 1985). PO is responsible for converting phenols to quinones, which then polymerize to produce melanin (González‐Santoyo and Córdoba‐Aguilar, 2012). Melanogenesis begins with the conversion of phenylalanine to tyrosine, after which PO hydroxylates tyrosine into

dihydroxyphenylalanine (DOPA) (González‐Santoyo and Córdoba‐Aguilar, 2012). PO then oxidizes DOPA into dopaquinone, which is converted into 5,6-dihydroxyindole (DHI) via two successive, non-enzymatic reactions (González‐Santoyo and Córdoba‐Aguilar, 2012). DHI is then oxidized by PO to produce indole-5,6-quinone, which polymerize to form melanin (González‐Santoyo and Córdoba‐Aguilar, 2012). An alternate mechanism of producing melanin involves DOPA being decarboxylated to form dopamine, PO then converts dopamine into dopaminequinone (figure 1.4).

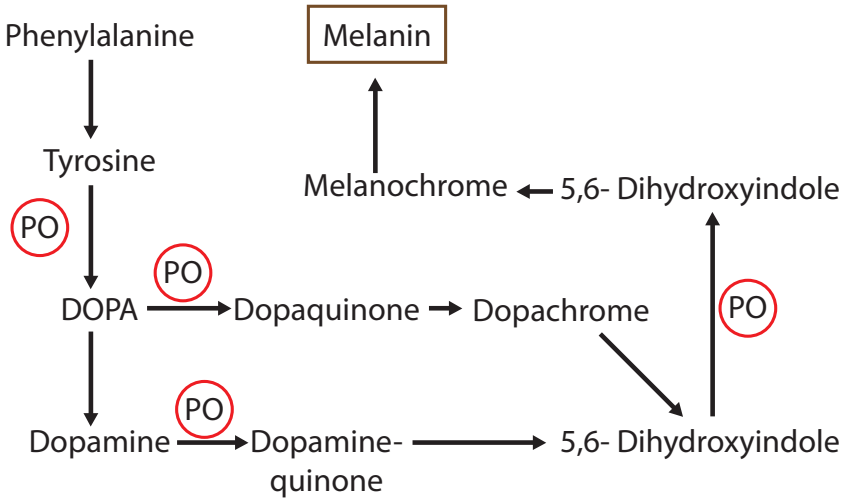

Figure 3.1: Schematic illustrating melanogenesis and the role of phenyloxidase (PO) in converting phenols to quinones (González‐Santoyo and Córdoba‐Aguilar, 2012).

Because PO plays a significant role in melanogenesis and encapsulation, its presence within the insect is indicative of a cellular immune response. Previous studies have examined the insect immune response to foreign bodies by measuring PO activity within haemolymph following implantation (Dubovskiy et al., 2013). Another approach to measuring insect immune response is by analyzing the amount of melanin deposited on a foreign object, such as nylon monofilaments and silica beads. The more melanin deposited on the foreign object, the stronger the immune response of the insect (Kivleniece et al., 2010; Nagel et al., 2011).

Encapsulation would be an issue for the FIETs developed in this study, as they would no longer be measuring the O_2 within the insect, but the O_2 within the cyst. Furthermore, any melanin deposited onto the FIET would reduce the transmittance of the excitation and emission wavelengths of the ratiometric dye system, thus rendering the bead useless.

The second concern of biocompatibility is the effects of the FIETs on the model insects' mortality and vitality. The question of whether any component in the FIETs is toxic needs to be answered before they are proposed as an alternative to fibre-optic probes. PDMS was chosen as the matrix for the FIETs due to its optical transparency and gas permeability (Er Qiang et al., 2014; Regehr et al., 2009). However, there is some concern regarding uncured PDMS oligomers leaching from the matrix into biological media as well as PDMS absorbing hydrophobic cell signaling molecules such as estrogen (Regehr et al., 2009). These effects have only been looked at when PDMS is used to form the microfluidic platform via soft lithography, but need to be investigated for implantable sensors as well (Berthier et al., 2012; Regehr et al., 2009).

Aside from biocompatibility, several other confounding factors within an *in vivo* system need to be accounted for within the FIETs measurements. For instance, temperature most certainly affects the degree of quenching that occurs, thus affecting the PO_2 measurements of the FIETs. Therefore, it will be important to investigate the response of the FIETs to graded temperatures. Furthermore, it will likely be necessary to hold implanted insects within a constant temperature during measurements, and ensure that the FIETs are calibrated at the same temperature as that of the measurements. Likewise, it will be important to minimize insects' exposure to ambient light, as this will cause photodegradation of the

FIETs. Other biologically relevant factors, such as pH, should be investigated to quantify their effects on the FIETs' readings of PO_2.

3.3 Concluding remarks

The goal of this thesis was to develop FIETs for the measurement of O_2 in small insects as an alternative to fibre-optic probes. Within my thesis I characterized these FIETs in terms of their uniformity, response to PO_2, and photodegradation, as well demonstrating their use within an autofluorescent system. When it comes to their response to PO_2 and demonstrated use, these FIETs perform well when compared to similar micro-sized O_2 sensors. Their response to PO_2 is linear and they can be used to produce meaningful measurements of a PO_2 gradient within agar. However, improvements need to be made regarding the uniformity and photodegradation of the FIETs. A simpler and more reliable microfluidic approach needs to be pursued, one that will ensure a PDI value of less than 3%. To minimize their invasiveness, the FIETs should ideally be much smaller than 70 μm, which could be achieved with a different microfluidic approach. To mitigate photodegradation, the intensity of the excitation light source should be measured and then modified to improve the longevity of the FIETs, in combination with the imaging requirements of the camera. With these improvements, attention can then be turned to preparing the FIETs for *in vivo* use and assessing their biocompatibility. Perfecting the FIETs for use *in vivo* will allow for the validation of conclusions made in previous research, such as the effectiveness of O_2 guarding within dampwood termites (Lighton and Ottesen, 2005), and also broaden the scope of possible research questions for future studies.

Bibliography

Amao, Y. (2003). Probes and polymers for optical sensing of oxygen. *Microchimica Acta* **143**, 1-12.

Bagchi, R., Gallery, R. E., Gripenberg, S., Gurr, S. J., Narayan, L., Addis, C. E., Freckleton, R. P. and Lewis, O. T. (2014). Pathogens and insect herbivores drive rainforest plant diversity and composition. *Nature* **506**, 85-88.

Bedlek-Anslow, J. M., Hubner, J. P., Carroll, B. F. and Schanze, K. S. (2000). Micro-heterogeneous oxygen response in luminescence sensor films. *Langmuir* **16**, 9137-9141.

Beebe, D. J., Mensing, G. A. and Walker, G. M. (2002). Physics and applications of microfluidics in biology. *Annual Review of Biomedical Engineering* **4**, 261-286.

Bélanger, M. C. and Marois, Y. (2001). Hemocompatibility, biocompatibility, inflammatory and in vivo studies of primary reference materials low-density polyethylene and polydimethylsiloxane: A review. *Journal of Biomedical Materials Research* **58**, 467-477.

Berthier, E., Young, E. W. K. and Beebe, D. (2012). Engineers are from PDMS-land, biologists are from polystyrenia. *Lab on a Chip* **12**, 1224-1237.

Bibette, J., Calderon, F. L. and Poulin, P. (1999). Emulsions: basic principles. *Reports on Progress in Physics* **62**, 969.

Bremond, N., Thiam, A. R. and Bibette, J. (2008). Decompressing emulsion droplets favors coalescence. *Physical Review Letters* **100**, 024501.

Brenner, P., Fleig, L.-M., Liu, X., Welle, A., Bräse, S. and Lemmer, U. (2015). Degradation mechanisms of polyfluorene-based organic semiconductor lasers under ambient and oxygen-free conditions. *Journal of Polymer Science Part B: Polymer Physics* **53**, 1029-1034.

Broder, J., Majumder, A., Porter, E., Srinivasamoorthy, G., Keith, C., Lauderdale, J. and Sornborger, A. (2007). Estimating weak ratiometric signals in imaging data. I. Dual-channel data. *Journal of the Optical Society of America A* **24**, 2921-2931.

Brodersen, K. P., Pedersen, O. L. E., Walker, I. R. and Jensen, M. T. (2008). Respiration of midges (Diptera; Chironomidae) in British Columbian lakes: oxy-regulation, temperature and their role as palaeo-indicators. *Freshwater Biology* **53**, 593-602.

Brune, A. (2014). Symbiotic digestion of lignocellulose in termite guts. *Nature Reviews Microbiology* **12**, 168-180.

Brune, A., Emerson, D. and Breznak, J. A. (1995). The termite gut microflora as an oxygen sink: microelectrode determination of oxygen and pH gradients in guts of lower and higher termites. *Applied and Environmental Microbiology* **61**, 2681-2687.

Butt, K. R. and Lowe, C. N. (2007). A viable technique for tagging earthworms using visible implant elastomer. *Applied Soil Ecology* **35**, 454-457.

Cao, Y., Lee Koo, Y.-E. and Kopelman, R. (2004). Poly(decyl methacrylate)-based fluorescent PEBBLE swarm nanosensors for measuring dissolved oxygen in biosamples. *Analyst* **129**, 745-750.

Chambon, F. and Winter, H. H. (1985). Stopping of crosslinking reaction in a PDMS polymer at the gel point. *Polymer Bulletin* **13**, 499-503.

Chapman, R. F. (2013). The Insects: Structure and Function. United States of America: Cambridge University Press.

Chown, Steven L., Gibbs, Allen G., Hetz, Stefan K., Klok, C. J., Lighton, John R. B. and Marais, E. (2006). Discontinuous gas exchange in insects: A clarification of hypotheses and approaches. *Physiological and Biochemical Zoology* **79**, 333-343.

Clapham, M. E. and Karr, J. A. (2012). Environmental and biotic controls on the evolutionary history of insect body size. *Proceedings of the National Academy of Sciences* **109**, 10927-10930.

Collier, B. B., Singh, S. and McShane, M. (2011). Microparticle ratiometric oxygen sensors utilizing near-infrared emitting quantum dots. *Analyst* **136**, 962-967.

Conchello, J.-A. and Lichtman, J. W. (2005). Fluorescence microscopy. *Nature Methods* **2**, 910-919.

Cutkomp, L. K., Desaiah, D., Cheng, E. Y., Vea, E. V. and Koch, R. B. (1976). The in vivo sensitivity of ATPases to DDT, DDE, and physical immobilization in American cockroaches. *Pesticide Biochemistry and Physiology* **6**, 203-208.

Demchenko, A. P. (2010). The concept of λ-ratiometry in fluorescence sensing and imaging. *Journal of Fluorescence* **20**, 1099-1128.

Dinh, H., Coman, G., Hurwood, D. A. and Mather, P. B. (2012). Experimental assessment of the utility of visible implant elastomer tags in a stock improvement programme for giant freshwater prawn (Macrobrachium rosenbergii) in Vietnam. *Aquaculture Research* **43**, 1471-1479.

Doggett, S. L., Orton, C. J., Lilly, D. G. and Russell, R. C. (2011). Bed bugs: The Australian response. *Insects* **2**, 96.

Doggett, S. L. and Russell, R. C. (2008). The resurgence of bed bugs, Cimex spp.(Hemiptera: Cimicidae) in Australia. In *Proceedings of the Sixth International Conference on Urban Pests*, vol. 6: Veszprem: OOK-Press Kft.

Dubovskiy, I. M., Whitten, M. M. A., Kryukov, V. Y., Yaroslavtseva, O. N., Grizanova, E. V., Greig, C., Mukherjee, K., Vilcinskas, A., Mitkovets, P. V., Glupov, V. V. et al. (2013). More than a colour change: insect melanism, disease. *Proceedings of the Royal Society of London B: Biological Sciences* **280**.

Dudley, R. (1998). Atmospheric oxygen, giant Paleozoic insects and the evolution of aerial locomotor performance. *Journal of Experimental Biology* **201**, 1043.

Dyer, O. (2015). Zika virus spreads across Americas as concerns mount over birth defects. *British Medical Journal* **351**.

Er Qiang, L., Jia Ming, Z. and Sigurdur, T. T. (2014). Simple and inexpensive microfluidic devices for the generation of monodisperse multiple emulsions. *Journal of Micromechanics and Microengineering* **24**, 015019.

Gaston, K. J. and Chown, S. L. (2013). Macroecological patterns in insect body size. In *Body size: Linking pattern and process across space, time and taxonomic group*, eds. F. A. Smith and S. K. Lyons), pp. 13-61. Chicago: The University of Chicago Press.

González‐Santoyo, I. and Córdoba‐Aguilar, A. (2012). Phenoloxidase: a key component of the insect immune system. *Entomologia Experimentalis et Applicata* **142**, 1-16.

Greenlee, K. J. and Harrison, J. F. (2004). Development of respiratory function in the American locust Schistocerca americana I. Across-instar effects. *Journal of Experimental Biology* **207**, 497-508.

Greenlee, K. J., Socha, J. J., Eubanks, H. B., Pedersen, P., Lee, W.-K. and Kirkton, S. D. (2013). Hypoxia-induced compression in the tracheal system of the tobacco hornworm caterpillar, Manduca sexta. *Journal of Experimental Biology* **216**, 2293-2301.

Groenewald, B., Hetz, S. K., Chown, S. L. and Terblanche, J. S. (2012). Respiratory dynamics of discontinuous gas exchange in the tracheal system of the desert locust, Schistocerca gregaria. *Journal of Experimental Biology* **215**, 2301-2307.

Hare, L. and Tessier, A. (1998). The aquatic insect Chaoborus as a biomonitor of trace metals in lakes. *Limnology and Oceanography* **43**, 1850-1859.

Harrison, J. F. (1989). Ventilatory frequency and haemolymph acid-base status during short-term hypercapnia in the locust, Schistocerca nitens. *Journal of Insect Physiology* **35**, 809-814.

Harrison, J. F. (2001). Insect acid-base phsyiology. *Annual Review of Entomology* **46**, 221-250.

Harrison, J. F., Kaiser, A. and VandenBrooks, J. M. (2010). Atmospheric oxygen level and the evolution of insect body size. *Proceedings of the Royal Society of London B: Biological Sciences* **277**, 1937-1946.

Harrison, J. F., Woods, A. H. and Roberts, S. P. (2012). Ecological and Environmental Physiology of Insects. New York: Oxford University Press Inc.

Hatjina, F., Papaefthimiou, C., Charistos, L., Dogaroglu, T., Bouga, M., Emmanouil, C. and Arnold, G. (2013). Sublethal doses of imidacloprid decreased size of hypopharyngeal glands and respiratory rhythm of honeybees in vivo. *Apidologie* **44**, 467-480.

Hodkinson, I. D. and Jackson, J. K. (2005). Terrestrial and aquatic invertebrates as bioindicators for environmental monitoring, with particular reference to mountain ecosystems. *Environmental Management* **35**, 649-666.

Hopf, H. W. and Hunt, T. K. (1994). Comparison of Clark electrode and optode for measurement of tissue oxygen tension. In *Oxygen Transport to Tissue XV*, pp. 841-847: Springer.

Hughes, V. A. and Douglas, P. (2006). Effect of lumophore and plasticiser concentration on the heterogeneity of oxygen quenching in thin film oxygen sensors. *Journal of Fluorescence* **16**, 403-409.

Inder, I. M. and Duncan, F. D. (2015). Gas exchange pattern transitions in the workers of the harvester termite. *Journal of Insect Physiology* **75**, 47-53.

Jia Ming, Z., Er Qiang, L. and Sigurdur, T. T. (2014). A co-flow-focusing monodisperse microbubble generator. *Journal of Micromechanics and Microengineering* **24**, 035008.

Jiang, K., Thomas, P. C., Forry, S. P., DeVoe, D. L. and Raghavan, S. R. (2012). Microfluidic synthesis of monodisperse PDMS microbeads as discrete oxygen sensors. *Soft Matter* **8**, 923-926.

Jörg, M., Simon, T., Roland, B., Khosro, S.-T., Barimani, H. V., Sebastian, S., Ulyshen, M. D. and Gossner, M. M. (2016). Protecting the forests while allowing removal of damaged trees may imperil saproxylic insect biodiversity in the hyrcanian beech forests of Iran. *Conservation Letters* **9**, 106-113.

Kansal, S. K., Singh, M. and Sud, D. (2007). Studies on photodegradation of two commercial dyes in aqueous phase using different photocatalysts. *Journal of Hazardous Materials* **141**, 581-590.

Kilpatrick, A. M. and Randolph, S. E. (2012). Drivers, dynamics, and control of emerging vector-borne zoonotic diseases. *The Lancet* **380**, 1946-1955.

Kivleniece, I., Krams, I., Daukšte, J., Krama, T. and Rantala, M. J. (2010). Sexual attractiveness of immune-challenged male mealworm beetles suggests terminal investment in reproduction. *Animal Behaviour* **80**, 1015-1021.

Klatt, B. K., Holzschuh, A., Westphal, C., Clough, Y., Smit, I., Pawelzik, E. and Tscharntke, T. (2014). Bee pollination improves crop quality, shelf life and commercial value. *Proceedings of the Royal Society of London B: Biological Sciences* **281**.

Klaus, A. V., Kulasekera, V. L. and Schawaroch, V. (2003). Three-dimensional visualization of insect morphology using confocal laser scanning microscopy. *Journal of Microscopy* **212**, 107-121.

Klimant, I., Ruckruh, F., Liebsch, G., Stangelmayer, A. and Wolfbeis, O. S. (1999). Fast response oxygen micro-optodes based on novel soluble ormosil glasses. *Microchimica Acta* **131**, 35-46.

Kloter, U., Schmid, H., Wolf, H., Michel, B. and Juncker, D. (2004). High-resolution patterning and transfer of thin PDMS films: fabrication of hybrid self-sealing 3D microfluidic systems. In *17th IEEE International Conference on Micro Electro Mechanical Systems. Maastricht MEMS 2004 Technical Digest*, pp. 745-748.

Koga, R., Tsuchida, T. and Fukatsu, T. (2009). Quenching autofluorescence of insect tissues for in situ detection of endosymbionts. *Applied Entomology and Zoology* **44**, 281-291.

Komai, Y. (2001). Direct measurement of oxygen partial pressure in a flying bumblebee. *Journal of Experimental Biology* **204**, 2999-3007.

Lakowicz, J. R. (2006). Principles of Fluorescence Spectroscopy. New York: Springer.

Lambert, R. C., Kolivras, K. N., Resler, L. M., Brewster, C. C. and Paulson, S. L. (2008). The potential for emergence of Chagas disease in the United States. *Geospatial Health* **2**, 227-239.

Lavine, M. D. and Strand, M. R. (2002). Insect hemocytes and their role in immunity. *Insect Biochemistry and Molecular Biology* **32**, 1295-1309.

Le Conte, Y. and Navajas, M. (2008). Climate change: impact on honey bee populations and diseases. *Revue scientifique et technique (International Office of Epizootics)*, 485-97, 499-510.

Li, Q., Han, X., Hou, J., Yin, J., Jiang, S. and Lu, C. (2015). Patterning poly(dimethylsiloxane) microspheres via combination of oxygen plasma exposure and solvent treatment. *The Journal of Physical Chemistry B* **119**, 13450-13461.

Lighton, J. R. B. and Ottesen, E. A. (2005). To DGC or not to DGC: oxygen guarding in the termite Zootermopsis nevadensis (Isoptera: Termopsidae). *Journal of Experimental Biology* **208**, 4671-4678.

Matsumoto, H., Tanaka, K., Noguchi, H. and Hayakawa, Y. (2003). Cause of mortality in insects under severe stress. *European Journal of Biochemistry* **270**, 3469-3476.

Matthews, P. G. D., Snelling, E. P., Seymour, R. S. and White, C. R. (2012). A test of the oxidative damage hypothesis for discontinuous gas exchange in the locust Locusta migratoria. *Biology Letters* **8**, 682-684.

Matthews, P. G. D. and Terblanche, J. S. (2015). Chapter One - Evolution of the Mechanisms Underlying Insect Respiratory Gas Exchange. In *Advances in Insect Physiology*, vol. Volume 49 (ed. J. Russell), pp. 1-24: Academic Press.

Matthews, P. G. D. and White, C. R. (2011a). Discontinuous gas exchange in insects: Is it all in their heads? *The American Naturalist* **177**, 130-134.

Matthews, P. G. D. and White, C. R. (2011b). Regulation of gas exchange and haemolymph pH in the cockroach Nauphoeta cinerea. *Journal of Experimental Biology* **214**, 3062-3073.

McDonagh, C., MacCraith, B. D. and McEvoy, A. K. (1998). Tailoring of sol−gel films for optical sensing of oxygen in gas and aqueous phase. *Analytical Chemistry* **70**, 45-50.

Moffatt, C. (2013). Using Visible Implant Elastomer to tag insects across life stages: a preliminary investigation with blow flies (Diptera: Calliphoridae). *The Canadian Entomologist* **145**, 466-470.

Nagel, L., Mlynarek, J. J. and Forbes, M. R. (2011). Immune response to nylon filaments in two damselfly species that differ in their resistance to ectoparasitic mites. *Ecological Entomology* **36**, 736-743.

Niven, J. E., Graham, C. M. and Burrows, M. (2007). Diversity and Evolution of the Insect Ventral Nerve Cord. *Annual Review of Entomology* **53**, 253-271.

Nurumbetov, G., Ballard, N. and Bon, S. A. F. (2012). A simple microfluidic device for fabrication of double emulsion droplets and polymer microcapsules. *Polymer Chemistry* **3**, 1043-1047.

Oliveira, C. M., Auad, A. M., Mendes, S. M. and Frizzas, M. R. (2013). Economic impact of exotic insect pests in Brazilian agriculture. *Journal of Applied Entomology* **137**, 1-15.

Peterson, S. L., McDonald, A., Gourley, P. L. and Sasaki, D. Y. (2005). Poly(dimethylsiloxane) thin films as biocompatible coatings for microfluidic devices: Cell culture and flow studies with glial cells. *Journal of Biomedical Materials Research Part A* **72A**, 10-18.

Piacentini, E., Drioli, E. and Giorno, L. (2014). Membrane emulsification technology: Twenty-five years of inventions and research through patent survey. *Journal of Membrane Science* **468**, 410-422.

Pimentel, M. A. G., Faroni, L. R. D. A., Tótola, M. R. and Guedes, R. N. C. (2007). Phosphine resistance, respiration rate and fitness consequences in stored-product insects. *Pest Management Science* **63**, 876-881.

Potts, S. G., Biesmeijer, J. C., Kremen, C., Neumann, P., Schweiger, O. and Kunin, W. E. (2010). Global pollinator declines: trends, impacts and drivers. *Trends in Ecology & Evolution* **25**, 345-353.

Quevedo, E., Steinbacher, J. and McQuade, D. T. (2005). Interfacial polymerization within a simplified microfluidic device: capturing capsules. *Journal of the American Chemical Society* **127**, 10498-10499.

R Development Core Team. (2010). R: A language and environment for statistical computing. Vienna, Austria: R Foundation for Statistical Computing.

Rainford, J. L., Hofreiter, M. and Mayhew, P. J. (2016). Phylogenetic analyses suggest that diversification and body size evolution are independent in insects. *Biomed Central Evolutionary Biology* **16**, 1-17.

Ratcliffe, N., Rowley, A., Fitzgerald, S. and Rhodes, C. (1985). Invertebrate immunity: basic concepts and recent advances. *International Review of Cytology* **97**, 350.

Rayleigh, L. (1878). On the instability of jets. *Proceedings of the London Mathematical Society* **s1-10**, 4-13.

Regehr, K. J., Domenech, M., Koepsel, J. T., Carver, K. C., Ellison-Zelski, S. J., Murphy, W. L., Schuler, L. A., Alarid, E. T. and Beebe, D. J. (2009). Biological implications of polydimethylsiloxane-based microfluidic cell culture. *Lab on a Chip* **9**, 2132-2139.

Reiter, P. (2014). Climate change and mosquito-borne disease: knowing the horse before hitching the cart. *Revue scientifique et technique (International Office of Epizootics)* **27**.

Schilman, P. E., Kaiser, A. and Lighton, J. R. B. (2008). Breathe softly, beetle: Continuous gas exchange, water loss and the role of the subelytral space in the tenebrionid beetle, Eleodes obscura. *Journal of Insect Physiology* **54**, 192-203.

Schneider, C. A., Rasband, W. S. and Eliceiri, K. W. (2012). NIH Image to ImageJ: 25 years of image analysis. *Nature Methods* **9**, 671-675.

Severinghaus, J. W. and Astrup, P. B. (1986). History of blood gas analysis. IV. Leland Clark's oxygen electrode. *Journal of Clinical Monitoring* **2**, 125-139.

Shah, R. K., Shum, H. C., Rowat, A. C., Lee, D., Agresti, J. J., Utada, A. S., Chu, L.-Y., Kim, J.-W., Fernandez-Nieves, A., Martinez, C. J. et al. (2008). Designer emulsions using microfluidics. *Materials Today* **11**, 18-27.

Snelling, E. P., Seymour, R. S., Runciman, S., Matthews, P. G. D. and White, C. R. (2011). Symmorphosis and the insect respiratory system: allometric variation. *Journal of Experimental Biology* **214**, 3225-3237.

Stork, N. E., McBroom, J., Gely, C. and Hamilton, A. J. (2015). New approaches narrow global species estimates for beetles, insects, and terrestrial arthropods. *Proceedings of the National Academy of Sciences* **112**, 7519-7523.

Taylor, P. (1998). Ostwald ripening in emulsions. *Advances in Colloid and Interface Science* **75**, 107-163.

Tomotika, S. (1935). On the instability of a cylindrical thread of a viscous Liquid surrounded by another viscous fluid. *Proceedings of the Royal Society of London. Series A - Mathematical and Physical Sciences* **150**, 322-337.

Tsuzuki, S., Matsumoto, H., Furihata, S., Ryuda, M., Tanaka, H., Jae Sung, E., Bird, G. S., Zhou, Y., Shears, S. B. and Hayakawa, Y. (2014). Switching between humoral and cellular immune responses in Drosophila is guided by the cytokine GBP. *Nature Communications* **5**, 4628.

Utada, A. S., Lorenceau, E., Link, D. R., Kaplan, P. D., Stone, H. A. and Weitz, D. A. (2005). Monodisperse double emulsions generated from a microcapillary device. *Science* **308**, 537-541.

Valledor, M., Campo, J. C., Sánchez-Barragán, I., Viera, J. C., Costa-Fernández, J. M. and Sanz-Medel, A. (2006). Luminescent ratiometric method in the frequency domain with dual phase-shift measurements: Application to oxygen sensing. *Sensors and Actuators B: Chemical* **117**, 266-273.

VandenBrooks, J. M., Munoz, E. E., Weed, M. D., Ford, C. F., Harrison, M. A. and Harrison, J. F. (2012). Impacts of paleo-oxygen levels on the size, development, reproduction, and tracheal systems of Blatella germanica. *Evolutionary Biology* **39**, 83-93.

Vladisavljević, G. T., Kobayashi, I. and Nakajima, M. (2012). Production of uniform droplets using membrane, microchannel and microfluidic emulsification devices. *Microfluidics and Nanofluidics* **13**, 151-178.

Wang, X.-d. and Wolfbeis, O. S. (2014). Optical methods for sensing and imaging oxygen: materials, spectroscopies and applications. *Chemical Society Reviews* **43**, 3666-3761.

Weisser, W. W. and Siemann, E. (2013). Insects and Ecosystem Function: Springer Science & Business Media.

Whitesides, G. M. (2006). The origins and the future of microfluidics. *Nature* **442**, 368-373.

Whitlock, M. and Schluter, D. (2015). The Analysis of Biological Data. Greenwood Village, Colorado: Roberts and Company Publishers.

Wigglesworth, V. B. (1930). A theory of tracheal respiration in insects. *Proceedings of the Royal Society of London. Series B, Containing Papers of a Biological Character* **106**, 229-250.

Wigglesworth, V. B. (1935). The regulation of respiration in the flea, Xenopsylla cheopis, Roths. (Pulicidae). *Proceedings of the Royal Society of London B: Biological Sciences* **118**, 397-419.

Wolfbeis, O. S. (2005). Materials for fluorescence-based optical chemical sensors. *Journal of Materials Chemistry* **15**, 2657-2669.

Wu, C., Bull, B., Christensen, K. and McNeill, J. (2009). Ratiometric single-nanoparticle oxygen sensors for biological imaging. *Angewandte Chemie International Edition* **48**, 2741-2745.

Wu, P., Wang, Y., Luo, Z., Li, Y., Li, M. and He, L. (2014). A 3D easily-assembled Micro-Cross for droplet generation. *Lab on a Chip* **14**, 795-798.

Xu, H., Aylott, J. W., Kopelman, R., Miller, T. J. and Philbert, M. A. (2001). A real-time ratiometric method for the determination of molecular oxygen inside living cells using sol−gel-based spherical optical nanosensors with applications to rat C6 glioma. *Analytical Chemistry* **73**, 4124-4133.

Yang, L. H. and Gratton, C. (2014). Insects as drivers of ecosystem processes. *Current Opinion in Insect Science* **2**, 26-32.

Appendices

Appendix A: Details of the imaging chamber

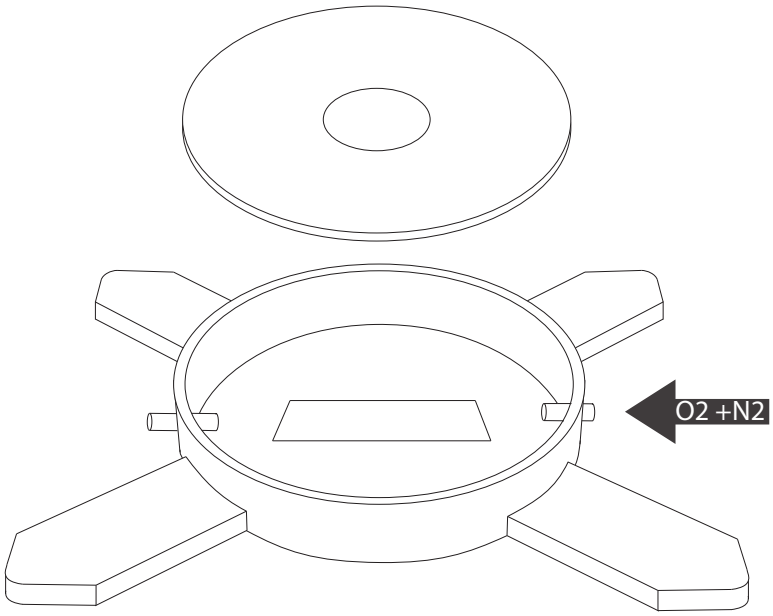

Figure A1: The imaging chamber designed for holding the FIETs within steady-state concentrations of oxygen. The inner diameter of the chamber measures 112 mm, the height of the chamber is 20 mm. A piece of clear plastic was epoxied into the center of the lid to allow transmitted light to enter the chamber.

Appendix B: FIET diameters produced in each chip

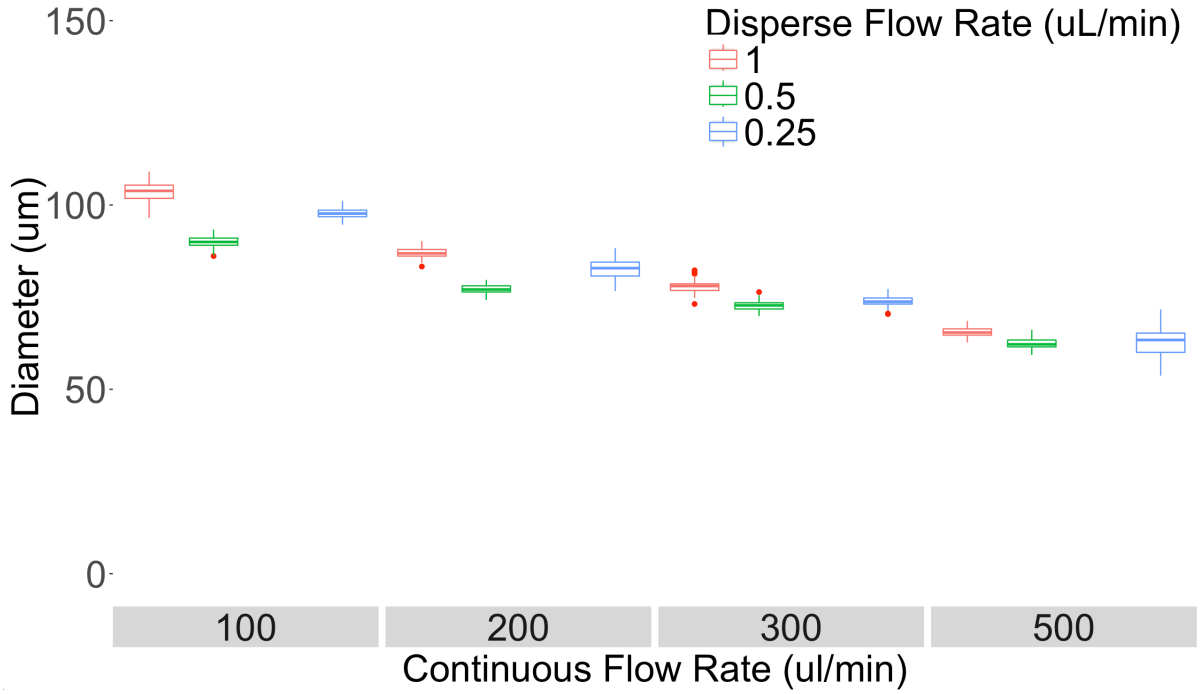

Figure B1: Average sizes of fluorescent implantable elastomer tags produced in the November 2nd microfluidic chip, outliers are indicated by red points. The disperse phase is 550 cSt polydimethylsiloxane and continuous phase is 5% Kolliphor.

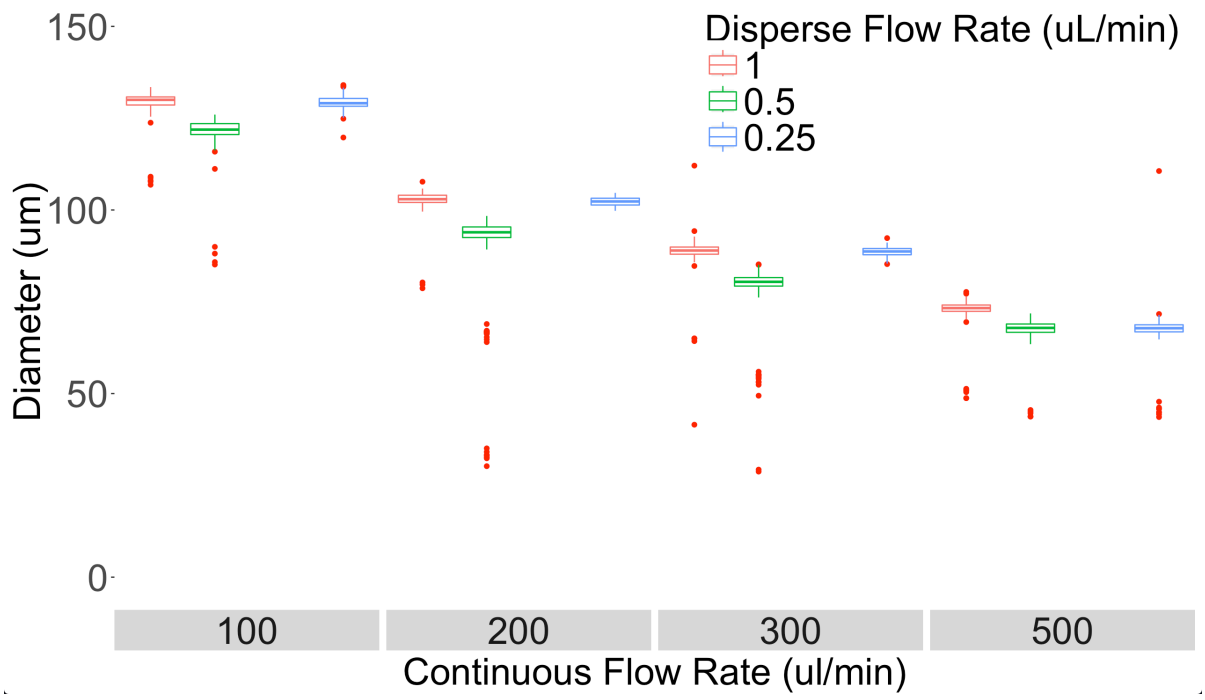

Figure B2: Average sizes and standard error of fluorescent implantable elastomer tags produced in the November 14th microfluidic chip, outliers are indicated by red points. The disperse phase is 550 cSt polydimethylsiloxane and continuous phase is 5% Kolliphor.

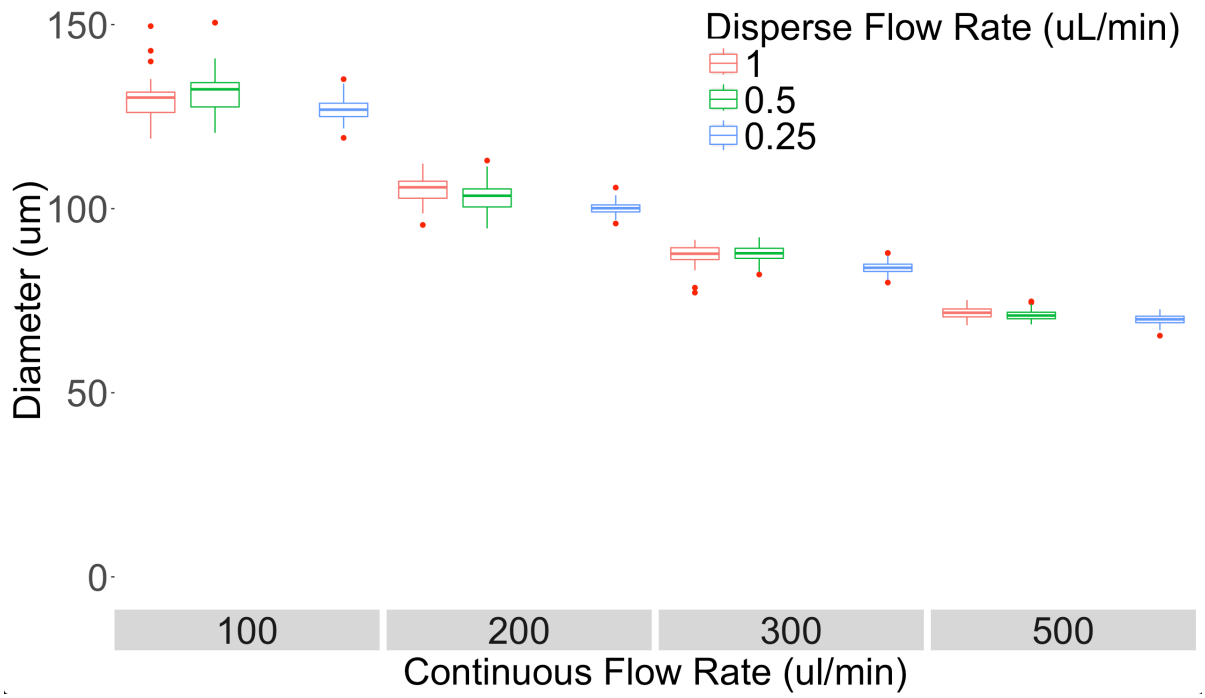

Figure B3: Average sizes and standard error of fluorescent implantable elastomer tags produced in the October 17th microfluidic chip, outliers are indicated by red points. The disperse phase is 550 cSt polydimethylsiloxane and continuous phase is 5% Kolliphor.

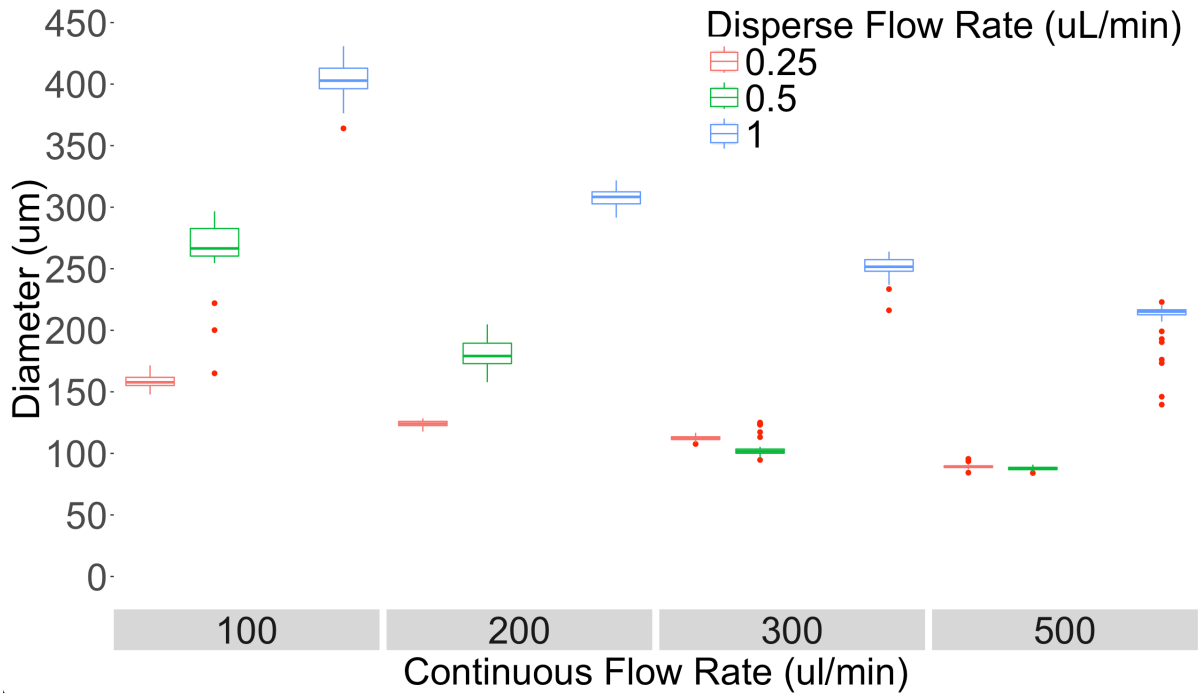

Figure B4: Average sizes and standard error of FIETs produced in the August 17th microfluidic chip, outliers are indicated by red points. The disperse phase is 550 cSt polydimethylsiloxane and continuous phase is 1% sodium dodecyl sulfate.

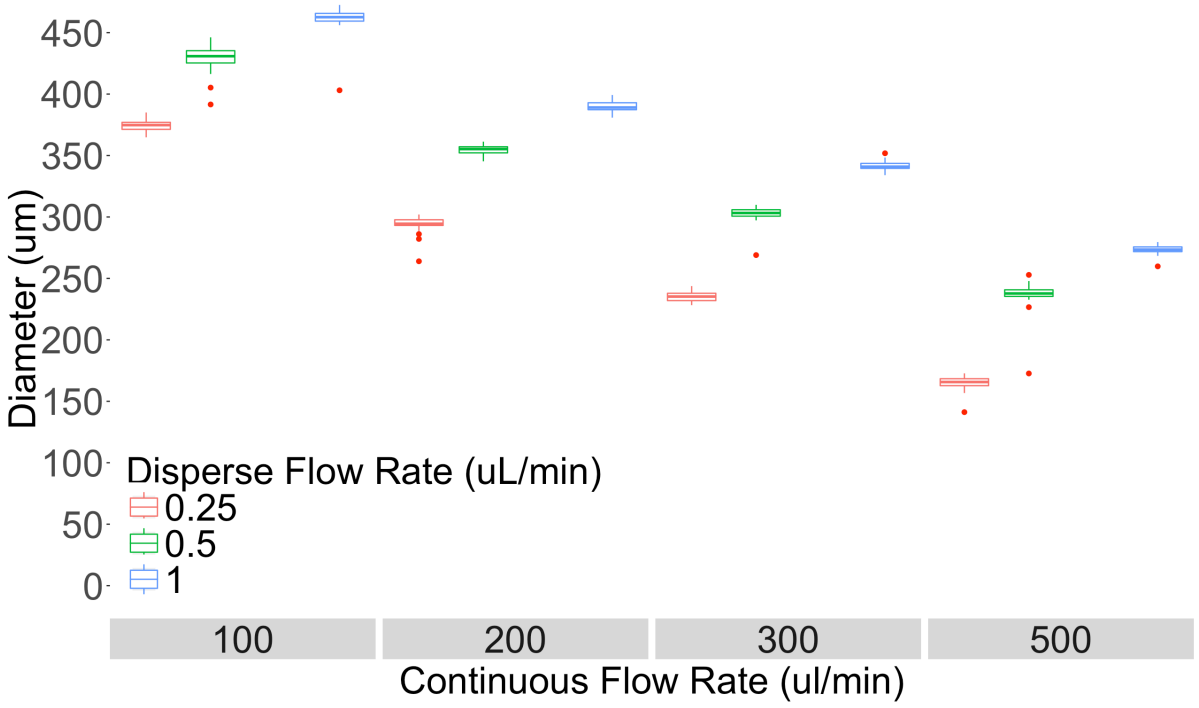

Figure B5: Average sizes and standard error of FIETs produced in the August 23rd microfluidic chip, outliers are indicated by red points. The disperse phase is 550 cSt polydimethylsiloxane and continuous phase is 1% sodium dodecyl sulfate.

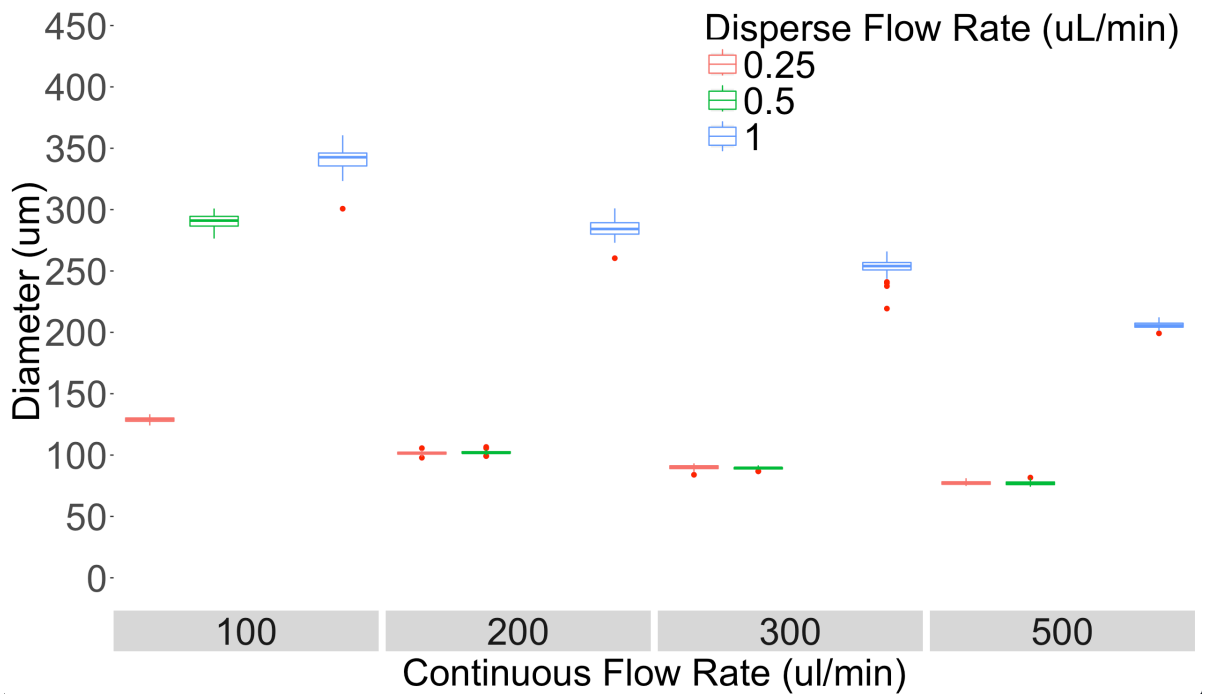

Figure B6: Average sizes and standard error of FIETs produced in the August 31st microfluidic chip, outliers are indicated by red points. The disperse phase is 550 cSt polydimethylsiloxane and continuous phase is 1% sodium dodecyl sulfate.

Appendix C: Photodegradation over 10 minutes

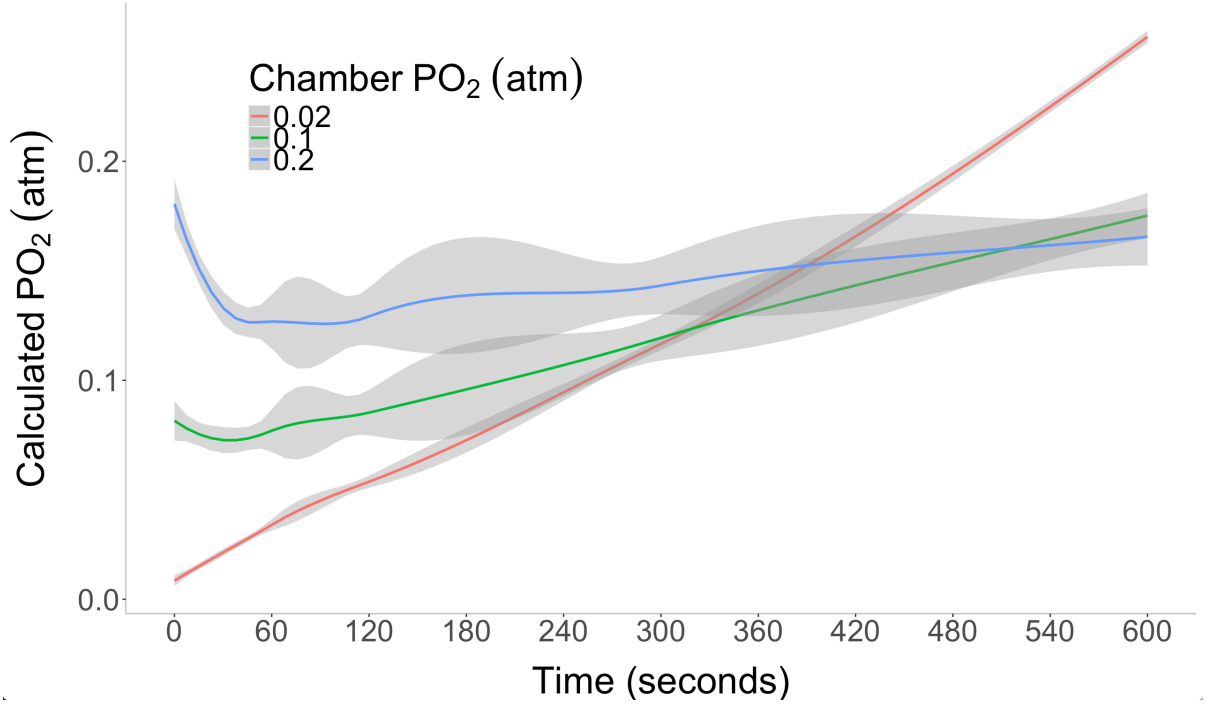

Figure C1: Photodegradation of FIETs with hydrated gas mixtures of 0.02, 0.1 and 0.2 atmospheres of oxygen in nitrogen over 10 minutes (600 seconds) of constant illumination with 390 nm light.

Appendix D: Details on the operation of the microfluidic chip

Multiple unforeseen issues arose during the development of the microfluidic chip, resulting in several changes to the chip design to ensure a uniform emulsion of FIETs. Firstly, design of the exit orifice of the injection tube required several iterations to optimize the uniformity and size of the FIETs produced. Using a micropipette puller, it was simple to create an injection tube with an exit orifice of 3 μm or less, which would theoretically produce FIETs of 10 μm in diameter or smaller. In reality, our lab is not a dust-free environment and having such a fine orifice resulted in clogging issues and non-functional microfluidic chips. To create an exit orifice between 5-10 μm, I tried pulling a fine tip and dragging the pulled microcapillary across a taut Kimwipe. This resulted in an uneven and large orifice (around 50 μm), and the microfluidic chips with this style of injection tube could only produce very large FIETs. Finally, I settled on an end orifice diameter of 13 μm using a micropipette puller. Clogging still remained an issue, albeit fixable with stringent cleaning and filtering, and the sizes of the FIETs produced were still within the desired range. In addition to a large exit orifice of the injection tube, I added a syringe filter on the disperse phase inlet port to reduce the amount of contaminants entering the chip. Clogging still occurred but was correctable by withdrawing the continuous phase via the injection tube orifice into an empty syringe placed at the disperse phase inlet. Even with the orifice of the injection tip optimized to its minimum, it proved difficult to produce FIETs under 50 μm in diameter.

Based on previous studies (Utada et al., 2005), I had originally planned to use a mixture of glycerol, water and surfactant as the continuous phase, as having a more viscous continuous phase increases the shear forces at the injection tube tip and thus leads to the

production of smaller droplets (Jia Ming et al., 2014; Utada et al., 2005). In addition, having a more viscous continuous phase contributes to a low Reynold's number, ensuring laminar flow (Beebe et al., 2002). However, previous studies have only used a glycerol-water mixture as the continuous phase when making micro-emulsions of silicon oil or gas (Er Qiang et al., 2014; Jia Ming et al., 2014). When glycerol was incorporated into the continuous phase of my microfluidic set-up, the resulting PDMS microspheres failed to cure. The mechanism behind glycerol inhibiting PDMS curing is unknown, and a literature search failed to find any studies investigating the matter. I then tried to make the continuous phase more viscous by increasing the percent mass of surfactant (SDS) within the continuous phase, but PDMS curing was once again inhibited. Finally, by switching to a polyethoxylated castor oil surfactant (Kolliphor), I was able to produce a highly viscous continuous phase and have the PDMS microspheres cure.